Journal of Science: Advanced Materials and Devices 10 (2025) 100966

Contents lists available at ScienceDirect

Journal of Science: Advanced Materials and Devices

journal homepage: www.elsevier.com/locate/jsamd

Research Article

Development of continuous fiber reinforced polymer composites using in-situ co-extrusion towpreg material extrusion process with optimized cooling and evaluation of their mechanical performance and quality

Nabeel Maqsood [a,b,*], Jawad Ullah [c,**], Marius Rimašauskas [d], Kateřina Skotnicová [a], Genrik Mordas [b], Conor McCrickard [c], Joamin Gonzalez-Gutierrez [e], Alistair McIlhagger [c], Edward Archer [c]

[a] Faculty of Materials Science and Technology, VSB – Technical University of Ostrava, 17. listopadu 2172/15, 708 00 Ostrava, Czech Republic
[b] 3D Technologies and Robotics Laboratory, Department of Laser Technologies, Center for Physical Sciences and Technology, Savanoriu Ave. 231, LT-02300, Vilnius, Lithuania
[c] School of Engineering, Ulster University, Belfast, Northern Ireland, BT15 1AP, UK
[d] Department of Production Engineering, Faculty of Mechanical Engineering and Design, Kaunas University of Technology, Studentu str. 56, LT-51424, Kaunas, Lithuania
[e] Lightweight Design and Simulations, Structural Composites Unit, Luxembourg Institute of Science and Technology (LIST), L-4940, Hautcharage, Luxembourg

ARTICLE INFO

Keywords:
In-situ Co-Extrusion with towpreg
Continuous fiber reinforced thermoplastic composites
Mechanical performance
X-ray micro-CT scan

ABSTRACT

Polymer composites mainly reinforced with continuous fibers manufactured using the material extrusion technique have gained attention due to their light weight and high-performance capabilities. Thermoplastics reinforced with continuous carbon fiber (CCF) offer exceptional mechanical properties. Polymer composites are fabricated using the material extrusion process, adapting various methods. Manufacturing such composites using fused filament fabrication (FFF) with high quality and reduced air void content is challenging due to the complexity of the process. In this study, in-situ co-extrusion with the towpreg process is used to manufacture CCF reinforced composites using the FFF technique. Two important printing parameters (layer thickness and line width) are considered. Mechanical properties (tensile, shear and compressive) were studied after the manufacturing of the composites. The porosity in the composites was observed using X-ray micro computed tomography scan, and the carbon fiber contents were estimated using the dissolution method, while the fracture analysis was performed using SEM. The results obtained suggested that both the printing parameters have a significant impact on the quality and mechanical properties of the additively manufactured composites. The polymer composite fabricated using a layer thickness of 0.4 mm and a line width of 1 mm showed the highest tensile, shear, and compressive strength of 364.69 MPa, 33.89 MPa, and 121.25 MPa, respectively, with a minimum porosity of 16.14 % and a reinforcement content of 26.12 % volume fraction. This thorough research gave insights into how differences in printing settings affect the structural integrity, mechanical properties, and quality of composites, directing future optimizations for improving the performance and quality of 3D-printed thermoplastic composites.

1. Introduction

Additive manufacturing (AM) or 3D printing is an advanced manufacturing process for fabricating parts layer upon layer using a 3D CAD model, following the printing parameters instructed by the software. AM technology is opposed to conventional or subtractive manufacturing processes; hence it is more sustainable and reliable. AM creates 3D objects having complex geometries with the minimum wastage of material, more accuracy, freedom in the geometrical shapes, a wide range for material selection, and economically at low production volumes [1,2]. These are some of the factors that qualify AM technologies to replace and overtake traditional and conventional

* Corresponding author. Faculty of Materials Science and Technology, VSB – Technical University of Ostrava, 17. listopadu 2172/15, 708 00 Ostrava, Czech Republic.
** Corresponding author.
E-mail addresses: nabeel.maqsood@ftmc.lt (N. Maqsood), j.ullah@ulster.ac.uk (J. Ullah).

https://doi.org/10.1016/j.jsamd.2025.100966
Received 9 June 2025; Received in revised form 17 July 2025; Accepted 3 August 2025
Available online 8 August 2025

manufacturing techniques. Fused Filament Fabrication (FFF) is one of the most widely used 3D printing technology for producing 3D objects using thermoplastic materials filaments as well as composite structures with discontinuous and continuous fibers [3–6]. Parts fabricated by pure thermoplastic materials using FFF 3D printers attain poor mechanical properties due to low strength and stiffness [7,8]. In order to improve its mechanical performance, reinforcement is introduced to the thermoplastic matrix material. Continuous carbon fiber (CCF) is a lightweight high strength material used as reinforcement for high structural applications. CCF possesses high strength compared to discontinuous fiber. Therefore it is recommended for high mechanical performance structures such as in the aerospace and automotive industry due to its exceptional strength-to-weight ratio [9,10]. However, production of continuous carbon fiber reinforced thermoplastic composites (CCFRTCs) using FFF technology with optimum printing parameters, controlled content of fiber, minimum air voids, and fine quality of the specimen, is one of the most challenging works in AM [1,11,12]. Printing parts with CCF is still one of the major challenges in the AM due to the complexity of the printing paths, orientations, and the bonding between the printing layers [13–15].

FFF is one of the most widely utilized material extrusion techniques for manufacturing thermoplastic composites reinforced with continuous fibers. To facilitate the integration of continuous fibers into the FFF process alongside thermoplastic extrusion, several advanced methods have been developed. These approaches include filament extrusion, towpreg extrusion, co-extrusion with towpreg, in-situ impregnation, in-situ consolidation, and inline impregnation processes [16–19]. A comparative study conducted by F. Wang et al. [20] evaluated the towpreg extrusion and in-situ impregnation techniques. The results demonstrated that the towpreg extrusion method enhanced the fiber volume fraction by approximately 7 % and reduced void content by about 6 %. This improvement translated into significant mechanical property enhancements, with tensile and flexural strengths of 3D-printed polymer composite structures increasing by 19 % and 20 %, respectively. These findings underscore the importance of fiber integration techniques in optimizing the mechanical performance of FFF-printed composites. To accommodate continuous fiber reinforcement, FFF 3D printers are often modified with specialized extrusion heads featuring dual input channels: one for continuous fiber and the other for thermoplastic filament. These channels converge into a single output nozzle, enabling the precise co-deposition of the matrix and reinforcement materials [15,21,22]. This innovative design facilitates the fabrication of continuous fiber-reinforced thermoplastic composites, leveraging the synergistic benefits of the high strength and stiffness of continuous fibers with the versatility and ease of processing offered by thermoplastic materials. It is well established that porosity levels in FFF-printed continuous fiber composites typically exceed those of traditional laminated composites, due to factors such as limited matrix infiltration, irregular fiber deposition, and the layer-wise nature of the process. Previous studies have reported porosity in the range of 20–30 % for similar material systems [11,23].

Printing parameters such as layer height, line width, extrusion multiplier, printing temperature, printing speed and fiber content have great influence on the mechanical performance as well as on the quality of the additively manufactured composite parts [21,24–26] and the physical appearance of the final product [21,27]. For example, M. Moradi et al. [28] indicated that the maximum failure load of PLA-bronze particle composite improved with higher layer thickness. PLA based short carbon and ABS composites filaments were considered with the printing parameters of layer height, printing orientation, infill density, nozzle diameter, nozzle temperature and raster angle to study their effect on electrical conductivity and mechanical properties [29–31]. On the other hand it has been demonstrated that flow rate multiplier had the strongest effect on tensile properties of FFF fabricated 17-4 PH stainless steel-composite specimens [32].

Less research has been performed on the fabrication of composite parts using continuous fiber reinforcing with improved quality and minimum air voids volume, and most of them have been focused on improving the mechanical performance with the optimum printing parameters [5,22,33–36]. Some research has also been performed by altering the printing parameters influencing on the mechanical performance of the continuous fiber composite structures to find the optimum solution [11,37–39]. H. Dou et al. [24] performed experimentation on the tensile properties of 3D printed 1K CCF-reinforced PLA composites by considering the printing parameters of layer height, line width, printing temperature, and printing speed. The results demonstrated that decreasing the layer height, line width and printing speed with higher printing temperature will have better mechanical properties. The optimum printing parameters reach a maximum tensile strength and tensile stiffness of 226.60 MPa and 22.38 GPa, respectively. K. Chen et al. [40] evaluated the optimum printing parameters (nozzle diameter, layer thickness, printing speed and temperature) of 3D-printed continuous glass fiber reinforced PLA composites on the mechanical properties and microstructure by achieving the maximum tensile strength of 241 MPa with 45 wt%. reinforcement content.

M Rimašauskas et al. [21] performed an investigation on the quality of 3D printed composite structures based on printing parameters (layer height and line width) for 1K impregnated CCF to reduce the void volume of the polymer composite structures. The experimental results showed that the composite specimen with a layer thickness of 0.3 mm and a line width of 1 mm had the smallest air void volume inside the specimen by achieving the maximum tensile strength of 183 MPa. Moreover, by reducing the layer thickness and line width, tensile strength increases, and higher amount of carbon fiber leads to better mechanical performance [24]. P. Zhuo et al. [12] fabricated continuous fiber composites with PA6 and investigated their mechanical performance by varying the volume fraction of fiber by reducing the air void content within the structures, that resulting in the best results with the fiber volume content of 44–47 % and the void content of 0.5–2.0 %. In previous research [41], a controlled cooling was provided to the composites during the fabrication process that results an improved in the composite printing quality as well as the mechanical performance considering the range of printing parameters, and the resulted that an increase of 17 % tensile strength and 25 % flexural strength was observed when compared to the composites that were fabricated without the use of cooling effect.

The motivation to simultaneously evaluate tensile, shear, and compressive properties arises from the target application areas of CCFRTCs, particularly in aerospace, automotive, and structural load-bearing components. These applications demand materials that exhibit multidirectional loading resistance. For instance, aerospace brackets, UAV structural ribs, and automotive crash panels encounter tensile loading during vibration and stretching, compressive forces under impact, and shear stresses at joint interfaces. Therefore, the holistic evaluation of these three mechanical behaviors offers a comprehensive understanding of the structural integrity and suitability of CCFRTCs under complex service conditions. The primary objective of this study is to investigate how variations in printing parameters affect the integrated mechanical behavior (tensile, shear, and compression) and structural quality (porosity and fiber content) of in-situ co-extruded CCFRTCs. This knowledge will inform process optimizations for achieving high-performance composite parts in real-world structural applications.

This manuscript delves into the intricacies of processing and manufacturing CCFRTC composites using FFF technology, systematically evaluating their mechanical performance and quality to address the growing demand for high-performance materials in industry and research. In this study, a modified FFF 3D printer with in-situ co-extrusion using the towpreg method was adapted to print the CCF composites with a thermoplastic matrix. An additional external controlled cooling was used to ensure the quality of the manufactured composites. For the fabrication of the polymer composites, two

important printing process parameters (layer thickness and line width) were considered and different values were used for the comparison. After the manufacturing, the mechanical performance was analyzed by performing tensile, shear, and compression testing. The composite's coupon's mechanical properties were also thoroughly compared with the pure PLA and PLA with short carbon fiber (PLA-SF) filaments. X-ray micro computed tomography (CT) scan was employed to observe the porosity within the composite structure, while the dissolution method was used to estimate the carbon fiber content in the fabricated specimens. After the mechanical testing, the composite specimen coupons were observed under scanning electron microscopy (SEM) to study the interface and fracture behavior. A theoretical model was also employed to predict the elastic modulus and tensile strength, and these predictions were compared with the experimental results to validate the model's accuracy. This comprehensive study provided valuable insights into the impact of varying printing parameters on the structural integrity and mechanical properties of CCFRTCs. The findings highlight the critical role of these settings in determining the performance and quality of 3D-printed composites. Such insights pave the way for future optimizations, enabling the development of advanced manufacturing strategies to enhance the mechanical performance, reliability, and overall quality of 3D-printed thermoplastic composite structures.

2. Materials and methods

2.1. Raw materials used for the fabrication of polymer composites

In this study, a polylactic acid (PLA) thermoplastic filament with a diameter of 1.75 mm, sourced from the PolyLite series by Polymaker, was employed as the matrix material. The selected PLA filament possesses a tensile strength of 46.6 MPa, an elastic modulus of 2.6 GPa, and a density of 1.24 g/cm^3. For reinforcement, standard 3K continuous carbon fiber (CCF) tow, specifically the T300B-3000 from Toray, was utilized. This CCF tow comprises 3000 carbon filaments, each with a diameter of 7 μm, and is derived from polyacrylonitrile. According to the manufacturer's specifications, the T300B-3000 CCF tow exhibits a tensile strength of 3530 MPa, a Young's modulus of 230 GPa, and a density of 1.76 g/cm^3. The XT-CF20 3D printing filament (ColorFabb) with a diameter of 1.75 mm was utilized. XT-CF20 is a composite filament made from thermoplastic reinforced with 20 % short carbon fibers (PLA-SF). This material exhibits a flexural modulus of 6.2 GPa and a tensile strength of 76 MPa.

Prior to composite fabrication, the standard CCF tow underwent a pre-treatment process involving impregnation with a 10 % weight solution of PLA 3D850 biopolymer, provided by NatureWorks, dissolved in methylene chloride (CH_2Cl_2) resin sourced from Eurochemicals. The purpose of this impregnation treatment was to enhance the printing process by improving inter-road and interlayer adhesion and, consequently, the mechanical properties of the composites. Previous studies have demonstrated that such impregnation treatments significantly affect the mechanical performance of composites, with higher concentrations of the impregnation solution being associated with superior print quality and enhanced mechanical properties in the final specimens [6].

2.2. Composites manufacturing process using FFF technology

In-situ co-extrusion with towpreg method was adapted to print the polymer composites, wherein the CCF was processed and combined with the matrix material (Fig. 1a). The composite feedstock was then introduced into the extrusion nozzle, enabling the simultaneous deposition of CCF and the PLA matrix material [39,42,43]. A custom-modified MeCreator 2 (Geeetech) FDM 3D printer was utilized for the experimental fabrication of composite specimens. This modification introduced two input channels: one for feeding the PLA thermoplastic filament and the other for the PLA-impregnated CCF. The impregnated CCF was directly fed into the extrusion nozzle via the extrusion head, while the PLA filament was driven into the same head by the drive wheel. Within the nozzle, the thermoplastic matrix melted and fused with the CCF, forming a composite bond that was extruded onto a borosilicate glass build platform. Key process parameters were maintained consistently throughout the experiments, including an extrusion multiplier of 0.7, a printing speed of 6 mm/s, a nozzle temperature of 230 °C, and a bed surface temperature of 90 °C.

The extrusion multiplier was set to 0.7 to compensate for the presence of embedded CCF, which displaces part of the matrix volume during co-extrusion. Preliminary trials showed that higher multipliers led to excessive material overflow, nozzle clogging, and dimensional inaccuracies due to over-extrusion in fiber-filled regions. In the previous study [41], an extrusion multiplier of 0.7 achieved more stable extrusion, proper fiber embedding, reduced porosity while preserving dimensional fidelity, and higher strength levels. While a print speed of 6

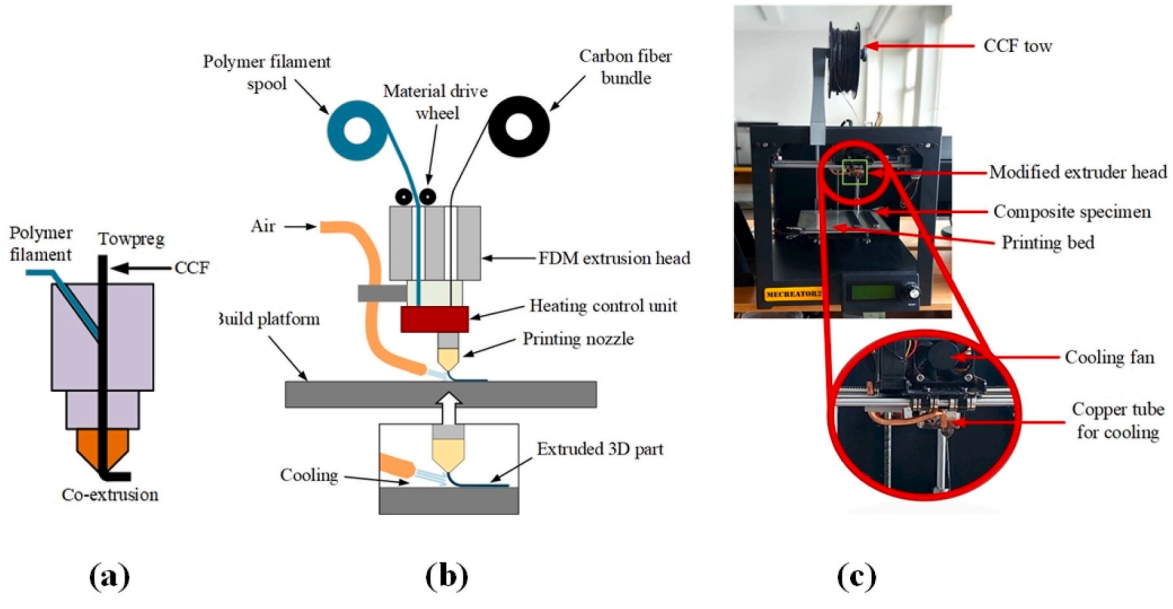

Fig. 1. Schematic of (a) co-extrusion with towpreg process, (b) the designed FDM 3D printer, (c) machine used for fabricating composite structures.

mm/s was selected to ensure consistent deposition and thermal bonding in the presence of continuous fibers. At higher speeds, deposition became unstable, and fiber placement accuracy degraded, especially during turns and infill transitions. The lower speed allowed sufficient time for the matrix to encapsulate the fiber and enhanced interfacial adhesion by maintaining localized thermal softening.

For all CCF composite specimen groups, slicing was performed using Simplify3D® (version 4.1.2), which provided customized control over line width, layer thickness, infill pattern, and print speed. The rectilinear toolpath and unidirectional print orientation were manually defined using custom G-code settings to align the fiber deposition along the loading direction (0°) for all mechanical tests. This ensured consistency in fiber alignment and allowed for accurate structure-property correlations. For the reference materials (PLA and PLA-SF), slicing was carried out using PrusaSlicer (version 2.5.0) with default optimized settings for the Prusa i3 MK3S printer, as outlined in Table 1.

It is important to note that the PLA and PLA-SF specimens were fabricated using standard FFF process parameters optimized for commercial filaments, while the PLA-CCF composite specimens were printed using a modified printer and in-situ co-extrusion process with specific parameters suitable for carbon fiber integration. Due to differences in printer hardware, feedstock type, and extrusion behavior (e.g., larger nozzle for PLA-CCF), printing parameters such as nozzle diameter, speed, and temperature could not be kept identical across all materials. Therefore, the PLA and PLA-SF results are presented solely as reference baselines to qualitatively assess the improvement in mechanical properties due to continuous fiber reinforcement, and not as direct parametric comparisons.

Table 1 presented the printing process parameters used for the fabrication of polymer and polymer composites. PLA and PLA-SF specimens were printed using Prusa i3 MK3S printer for the comparison with the composites with CCF.

The major modification performed during the experiment was introducing the controlled air flow cooling through pressure regulator. The reason for such modification is to ensure the high quality and fine fabrication of CCFRTC structures [41]. The copper tube was attached near the printing nozzle that enables the extruded composite to be uniformly printed on the built surface. Fig. 1a and b shows the schematic view of the modified designed FDM and the MeCreator 2 3D printer used for fabricating composite structure. The flow rate of the compressed air cooling was controlled through the digital pressure regulator valve. The cooling was controlled under the air flow rate of 40 l/m and kept constant till the part is fabricated completely. The point direction of the copper tube is directly towards the bed surface and the pointed towards the composite extruding through the printing nozzle that guides the extruded material and solidify it as it lays on the borosilicate glass and ensures that the composite placed on it instantly and during the curve made for another line, it solidifies and within the projected path and didn't drag and displaced the printing path. For the experimental research, 0° unidirectional composite specimens were printed with a rectilinear 100 % infill pattern.

Although elevated temperatures promote interlayer diffusion in conventional thermoplastic FFF, the integration of CCF imposes additional challenges related to fiber distortion, path deviation, and resin accumulation. In this co-extrusion setup, a controlled external airflow cooling system was employed to locally stabilize the extrudate immediately after deposition, not to cool the entire print environment. The purpose was to reduce drag-induced distortion caused by the fiber tension and ensure precise fiber steering and matrix placement, particularly around curved regions. This stabilization minimizes fiber buckling and misalignment, which are common in CCF printing.

Table 1
Printing process parameters for the experimentation used to fabricate specimens.

Parameters	3D Printers types		
	MeCreator 2	Prusa i3 MK3S	
	PLA-CCF	PLA	PLA-SF
Nozzle Diameter	1.5 mm	0.4 mm	0.4 mm
Extrusion Multiplier	0.7	1	1
Layer height	0.4–0.5 mm	0.2 mm	0.2 mm
Printing Speed	6.0 mm/s	25 mm/s	25 mm/s
Extruder temperature	230 °C	210 °C	250 °C
Bed temperature	90 °C	70 °C	80 °C
Fan Speed	60 %	30 %	30 %
External cooling	40 l/min	–	–
Internal/External fill pattern	Rectilinear	Aligned Rectilinear	Aligned Rectilinear
Infill percentage	100 %	100 %	100 %

2.3. Mechanical testing

Tensile, shear and compression tests were conducted to examine and determine the properties of 3D printed polymer composite specimens. Effects on the tensile properties (tensile strength and Young's modulus), shear properties (shear strength and shear modulus) and compressive properties (compressive strength and compressive modulus) of specimens were experimentally investigated. In the present study, ASTM D3039, ASTM D5379 and ASTM D695 standards were used to perform the tensile, shear and compression tests, respectively. In total, 90 samples were printed for the mechanical testing. All the tests were performed using a universal testing machine of Tinius Olsen H25KT having capacity of 25 kN at room temperature. Fig. 2 displays the CCFRTC specimens fabricated using FFF with the dimensions for tensile test, shear test and compression test.

2.3.1. Tensile testing

For the tensile testing, solid composite specimens with a rectangular cross-section were fabricated, measuring 150 mm in length, 13 mm in width, and 6 printed layers in thickness. To ensure a secure grip during testing, tabs were affixed to both ends of the specimens. These tabs were also 3D printed using PLA material, with dimensions of 50 mm in length, 12.5 mm in width, and 2 mm in thickness, featuring a bevel angle of 30°. Four strain measurement points were marked on the surface of each printed specimen, spaced 15 mm apart from the center, to assess the elastic strain during testing. The tensile test was conducted at a constant head displacement rate of 2 mm/min. At least 5 specimens were printed for each group to perform the experiment. The tensile stress of the composite specimens was calculated based on the applied load and the cross-sectional area, using the appropriate mathematical relationship for tensile stress evaluation.

$$\sigma_t = \frac{F}{bd} \tag{1}$$

Where, σ_t is the tensile stress (MPa), F is the maximum tensile load before failure (N), b is the width (mm) and d is the thickness of the composite specimen (mm).

2.3.2. Shear testing

For the shear test, composite specimens with a rectangular cross-section, measuring 76 mm in length, 20 mm in width, and 2.5 mm in thickness, were 3D printed. PLA tabs, measuring 32 mm in length, 20 mm in width, and 1.5 mm in thickness, were attached at each end of the specimen to ensure secure gripping during testing. Two V-notches, each with a 90° angle, were machined at the center of the specimen on both sides, spaced 12 mm apart from the tips of the notches. Strain gauges were affixed to the specimens to capture strain displacement throughout the testing process. The test was conducted at a constant head displacement rate of 2 mm/min. To ensure statistical reliability, at least five specimens were printed and tested for each experimental group, and

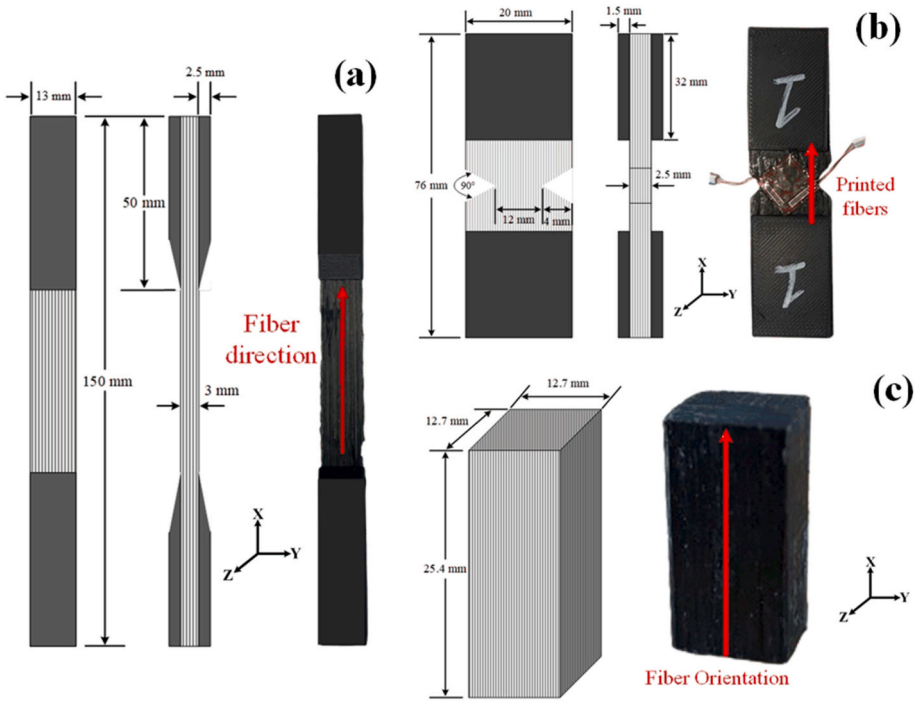

Fig. 2. CCFRTC specimens fabricated using FFF with dimensions for (a) tensile test, (b) shear test, (c) compression test.

the average values were used for analysis. The shear stress of the 3D printed composite specimens was calculated using the appropriate mathematical relationship for shear stress determination.

$$\tau_i = \frac{P}{A} \tag{2}$$

Where, τ_i is the shear stress (MPa), P is the maximum load (N) and A is the cross-sectional area of the composite specimen (mm^2).

2.3.3. Compression testing

For the compression test, composite specimens were fabricated in the form of rectangular blocks with dimensions of 25.4 mm × 12.7 mm × 12.7 mm. The CCFRTC specimens were initially printed with an extended length, which was then sectioned into three equal lengths, as recommended by the testing standards. The compression test was conducted with the crosshead speed controlled at 1.3 mm/min. Compressive force was applied in the direction parallel to the printed layers of the composite. For each experimental group, five specimens were manufactured and tested to ensure accurate and reliable results.

Fig. 3 presented the mechanical testing equipment used for the tensile test, shear test and compression test.

2.4. X-ray micro-CT scan analysis

Micro-computed tomography (micro-CT) analysis of the 3D-printed polymer composite specimens was performed using a Bruker SkyScan 1275 system (Bruker, USA). The scanner operated in microfocus mode

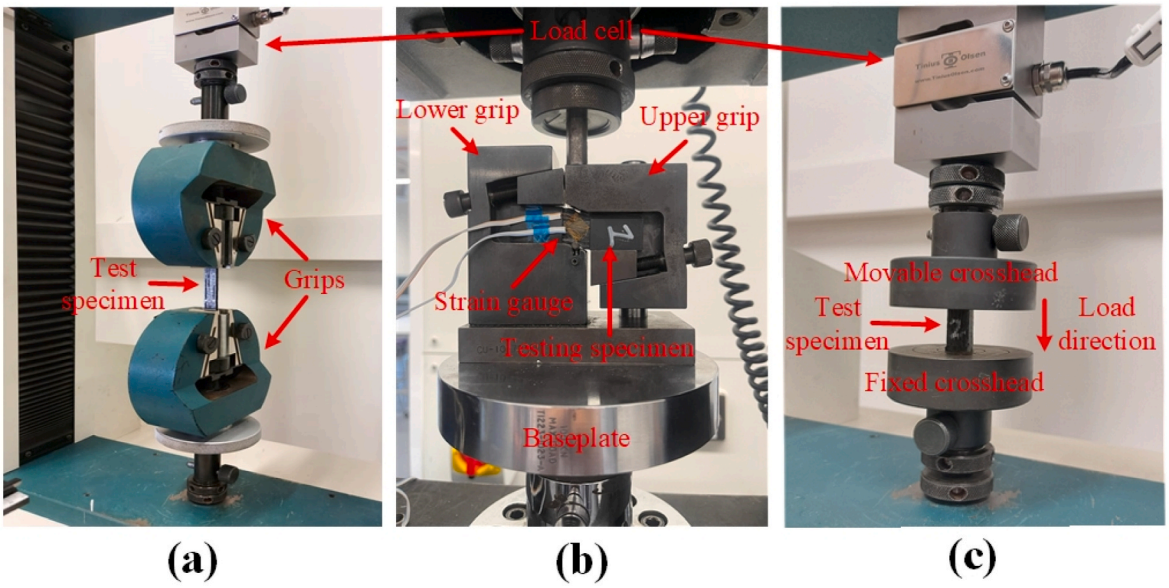

Fig. 3. Mechanical testing equipment for (a) tensile test, (b) shear test and (c) compression test.

with a cone-beam X-ray source set at 100 kV and 200 μA, and an integration time of 2000 ms. A total of 2970 projections were acquired over a full 360° rotation, using a 2048 × 2048 detector array with an active area of 410 × 410 mm^2, achieving an isotropic voxel resolution of 10 μm. A rotation step of 0.3° and a 0.5 mm aluminum filter were applied to reduce beam hardening effects. The reconstructed tomographic dataset for each sample consisted of 950 × 950 × 1600 voxels, processed using NRecon software (v1.7.4.6). Quantitative porosity analysis was conducted in CTAn (Bruker), while 3D visualization and phase segmentation were carried out in Dragonfly (Object Research Systems, ORS). A grey level threshold (GLT) was applied to separate solid from air phases, and the Otsu method was used for void binarization. To distinguish among matrix, fiber, and void regions, a combination of grayscale thresholding and region-growing algorithms was implemented [44]. While the 10 μm voxel resolution may not fully capture submicron pores or individual fiber boundaries, the segmentation protocol provided sufficient fidelity for identifying macro- and meso-scale voids and structural features. The x-ray CT scan test to detect the porosity within the 3D printed polymer composite structures were performed on the specimen block with the dimension of 30 x 10 × 10 mm^3. Three samples were taken into account for each set of composite groups to perform the experiment and the average value was considered. Fig. 4 shows the composite specimen block used for the CT scan and X-ray micro-CT scan machine used for the experimentation.

2.5. Reinforcement content determination in composite specimen using dissolution method

To estimate and calculate the carbon fiber content in the CCFRTC parts, the ASTM D 3171 standard procedure, "Standard Test Methods for Constituent Content of Composite Materials," was followed. Specifically, Method I was employed to determine the reinforcement content. In this method, the matrix material of the composite specimens is physically removed through chemical digestion, leaving the reinforcement fibers intact, which enables the calculation of fiber and matrix content. Following the standard protocol, three specimens from each group were tested to determine the reinforcement content. The procedure for measuring the carbon fiber content in the composite is illustrated in Fig. 5. Composite specimen blocks were 3D printed with initial dimensions of 120 × 10 × 10 mm^3. These samples were then sectioned into three equal parts, each with an average dimension of 35 × 10 × 10 mm^3, for the testing.

The samples were polished to eliminate surface roughness, thereby reducing potential measurement errors. In accordance with the standard, three specimens from each group were tested to determine the reinforcement content. To dissolve the matrix material for constituent content analysis, Procedure B was employed, which involved the use of a sulfuric acid and hydrogen peroxide solution. Following digestion, the remaining carbon fiber was thoroughly rinsed with distilled water and then placed in a universal oven (UFB 400, Memmert) at 100 °C for 3 h to ensure complete drying. Afterward, the dried CCF reinforcement was weighed using precision balance scales (ADJ 200-4, Kern) with an accuracy of ±0.1 mg. The densities of both the thermoplastic matrix and CCF reinforcement, as provided by the manufacturer, were used in subsequent calculations. Finally, the reinforcement content was calculated using the following expression, which accounts for the weight of the unaffected reinforcement and the matrix density.

$$W_r = \left(\frac{M_f}{M_i}\right) * 100 \tag{3}$$

where, W_r is weight percentage of reinforcement, M_i is the initial mass (g) of the specimen, and M_f is the final mass (g) of the specimen after digestion.

$$V_r = \left(\frac{M_f}{M_i}\right) * 100 * \frac{\rho_c}{\rho_r} \tag{4}$$

where V_r is volume percentage of reinforcement content, ρ_r is the density of the reinforcement, ρ_c (g/mL) is density of the composite specimen.

2.6. Fracture interface study analysis

The adhesion between the matrix and reinforcement is critical in determining the quality and performance of composite materials. To evaluate this aspect, a fracture analysis of the composites was conducted following the tensile testing. The focus of this study was to investigate the fracture interface between the thermoplastic matrix and the CCF reinforcement, specifically examining how these components separated under tensile loading and identifying the points at which they bonded together. Field emission scanning electron microscopy (FE-SEM, SU5000, Hitachi Co., Tokyo, Japan) was employed to capture micrograph images, facilitating a detailed analysis of the interfacial behavior of the matrix and reinforcement. This analysis provided insights into the mechanical interactions at the interface and the overall effectiveness of the adhesion between the fiber and matrix.

2.7. Theoretical model for the prediction of modulus of elasticity and tensile strength

The Rule of Mixtures (ROM) was employed to predict the elastic modulus and tensile strength of additively manufactured CCFRTC produced with varying layer heights and line widths. Changes in these printing parameters significantly influenced the tensile properties of the composites, resulting in diverse mechanical performance across the different groups. Each composite group exhibited unique elastic modulus values despite being fabricated using the same thermoplastic matrix and carbon fiber reinforcement. This variability can be attributed to differences in internal structure and fiber alignment induced by the layer height and line width variations. According to the ROM, the pre-

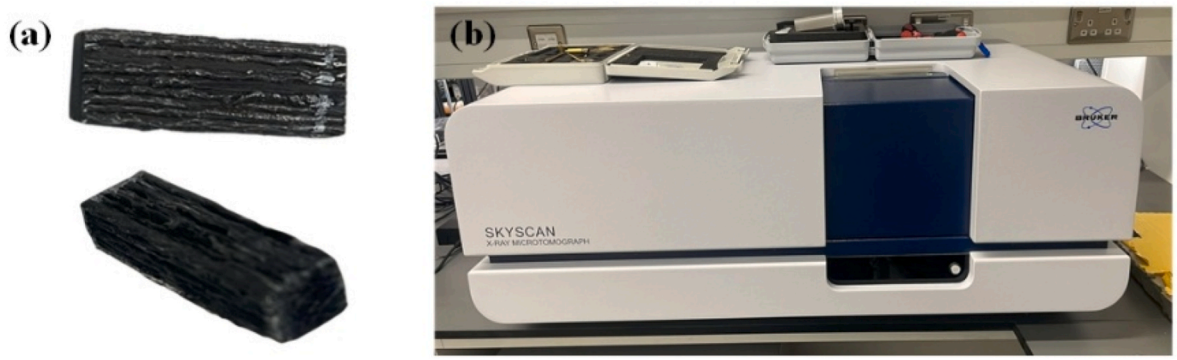

Fig. 4. (a) CCFRTC block manufactured using FFF for CT scan, (b) X-ray micro-CT scan machine.

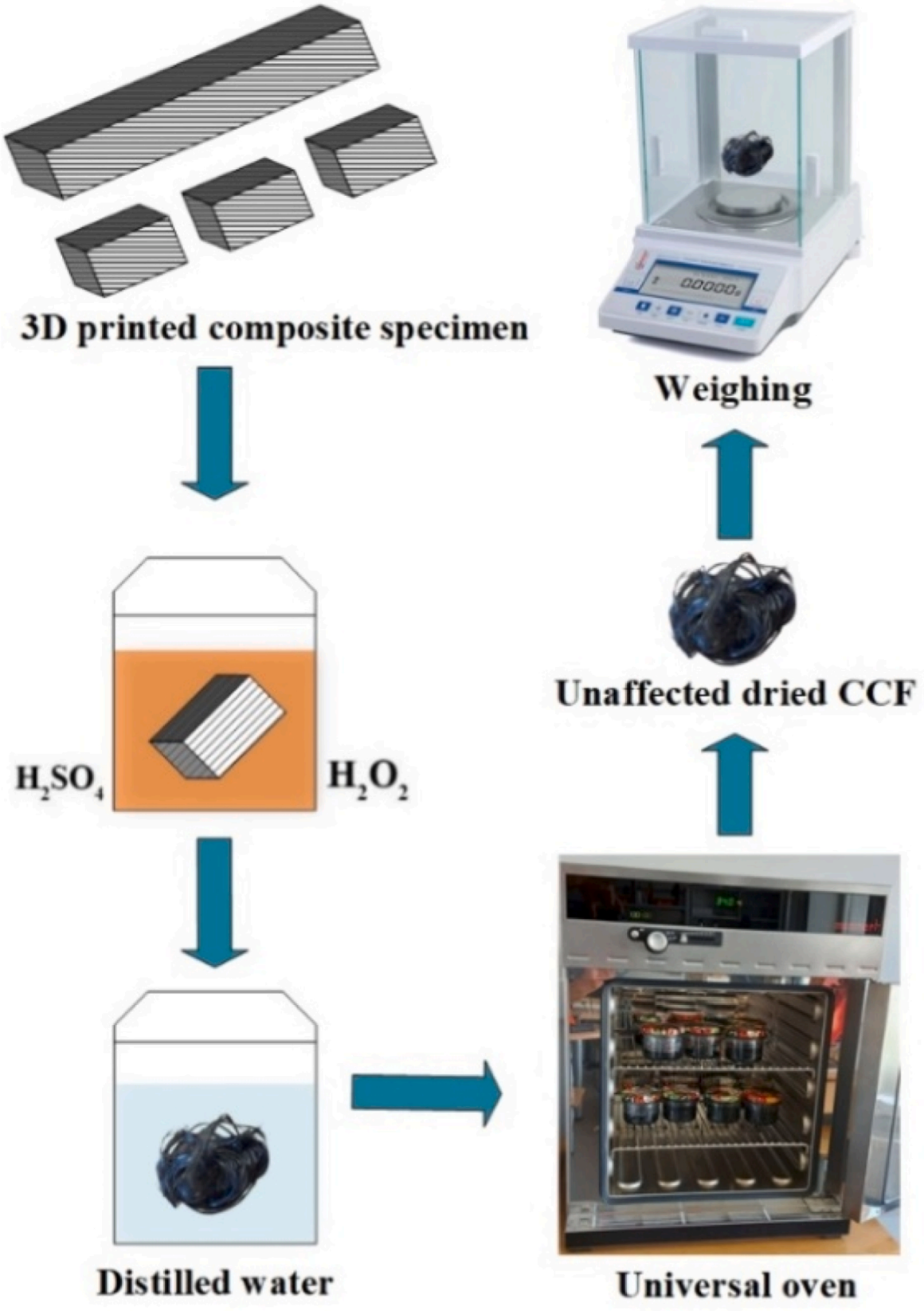

Fig. 5. Dissolution process for carbon fiber content determination.

dicted Young's modulus (E_c) and tensile strength (X_c) of fiber-reinforced composites were determined which account for the contributions of both the fiber and matrix phases [45]. These predictions help establish a theoretical baseline for comparison with experimentally measured mechanical properties.

The V_v in a composite material represents the volume of the empty space within the material. To incorporate the V_v in the ROM, one approach is to modify the formula to include the V_v fraction, which is the ratio of the V_v to the total volume of the composite. In the ROM, it can be included by adjusting the volume fractions of the constituent materials. To include the V_v in the ROM, the volume fraction of the voids must be considered. This can be done by adjusting the volume fractions of the constituent materials so that to take into account the volume occupied by the voids. The modified ROM formula for the E_c and X_c would be:

$$V_f + V_m + V_v = 1 \tag{5}$$

$$E_c = E_f(1 - V_m - V_v) + E_m(1 - V_f - V_v) \tag{6}$$

$$X_c = X_f(1 - V_m - V_v) + X_m(1 - V_f - V_v) \tag{7}$$

where.

V_f – volume fraction of the fiber;
V_m – volume fraction of the matrix;
V_v – volume void in the composite;
E_m – elastic modulus of the PLA matrix;
E_f – elastic modulus of CCF.
X_m– tensile strength of the PLA matrix
X_f – tensile strength of CCF

This approach, known as the Equal Strength Analysis (ESA) model, is built upon three key assumptions: (a) the material exhibits linear elastic behavior up to failure, (b) the longitudinal strain is equal across the fiber, matrix, and composite, and (c) the matrix contributes minimally to the load-carrying capacity after fiber failure [46].

3. Results and discussion

3.1. Mechanical tests analysis

Mechanical testing was performed to examine and determine the properties of 3D printed polymer composite specimens. Tensile properties (tensile strength and Young's modulus), shear properties (shear strength and shear modulus) and compressive properties (compressive strength and compressive modulus) of the CCFRTCs were experimentally investigated.

3.1.1. Tensile properties

Tensile test was performed to study the tensile properties (tensile strength and Young's modulus) of the manufactured polymer composites. The tensile stress-strain curves of the composite groups with the comparison of pure polymer and PLA-SF composite are presented in

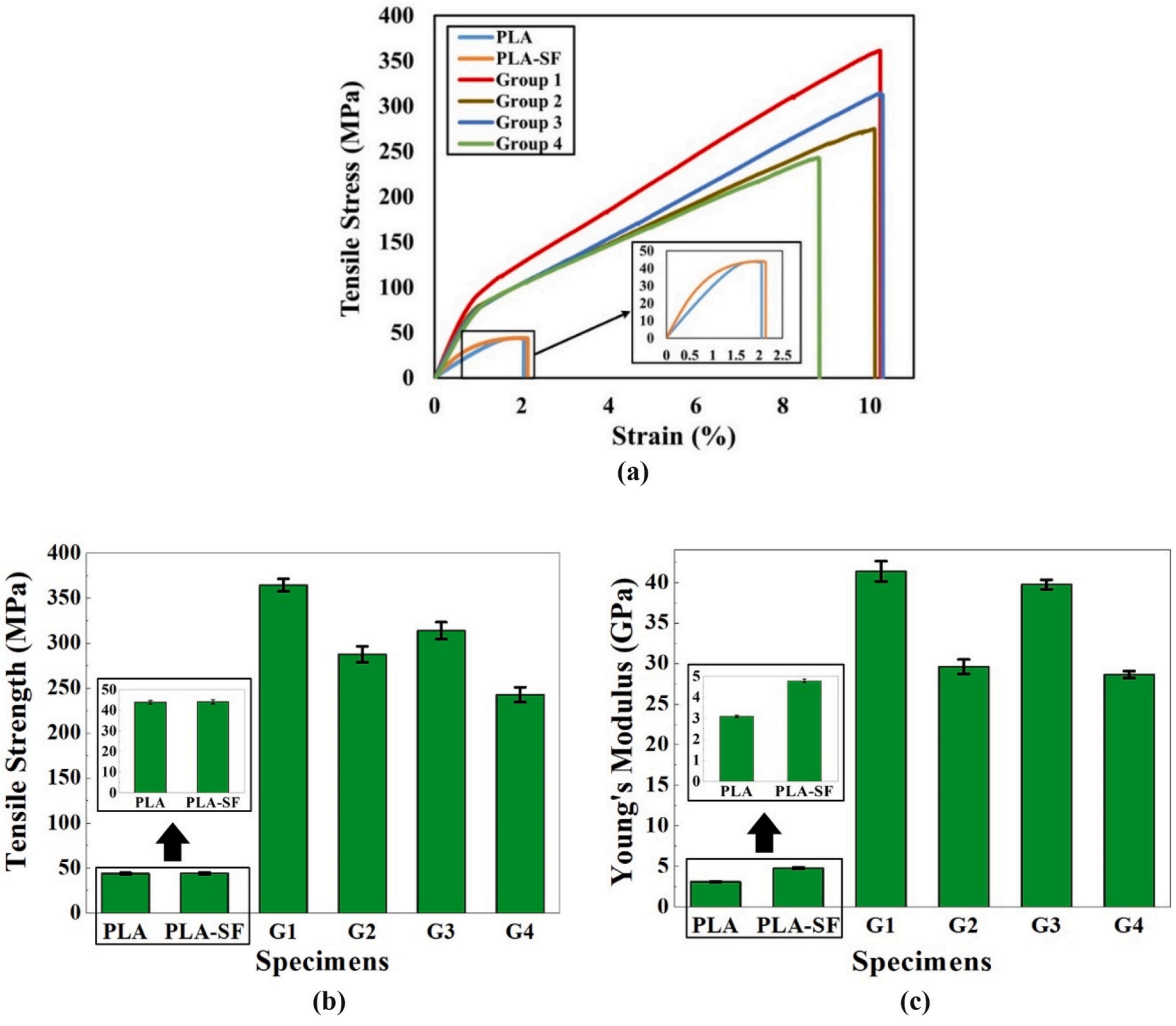

Fig. 6. Tensile properties of the CCFRTC's groups fabricated using FFF (a) tensile stress-strain curves, (b) tensile strength, (c) Young's modulus.

Fig. 6a. The tensile stress strain curves revealed that pure PLA material attains the lowest stress level and similar to that of PLA-SF composite specimen. The PLA and PLA-SF material curves showed a linear behavior initially, indicating elastic deformation, followed by a yield point and a relatively sharp drop after the peak, suggesting a brittle failure without significant plastic deformation.

Regarding the layer height and line width (Table 2), G1 composite material specimens reached the highest stress level among all the groups indicating the strongest material followed by G3, G2 and G4. It was observed that a reduction in layer thickness and line width leads to an increase in tensile stress levels. Both printing parameters directly influence the tensile stress behavior of the composite specimens.

The tensile properties (tensile strength and Young's modulus) are illustrated in Fig. 6b and c, respectively. From the obtained results, it was observed that the lowest tensile strength of 43.83 MPa was seen in pure PLA material specimen, while PLA-SF showed strength of 44.08 MPa which showed almost similar strength compared PLA. In comparison among the composite specimens printed with continuous fibers, the G4 specimen printed with layer thickness of 0.5 mm and line width of 1.2 mm showed the minimum tensile strength of 242.87 MPa. G2 and G3 exhibits the tensile strength of 287.48 MPa and 314.11 MPa, respectively, while G1 printed with layer thickness of 0.4 mm and line width of 1.0 mm reached the highest tensile strength of 364.69 MPa. G4 showed an increase in the tensile strength 5.5 times compared to pure PLA and PLA-SF material, while G1 showed 8.5 times higher strength compared to PLA and PLA-SF specimen which exhibits an increase of the tensile strength by approximately 730 %. The results also suggested that by decreasing the layer thickness and line width, the tensile strength increases and in comparison, to both the parameters, layer thickness showed more significant importance when discussing the tensile properties. G1 has shown an increase in the tensile strength by 50 % when compared to G4 composite specimen. When considering the layer thickness of 0.4 mm in G1 and G3, an increase in the strength level by 16 % was observed in G1. While in G3 when the layer thickness was kept lower (0.4 mm) with 1.2 mm line width in comparison to G2 where the line width was 1 mm with the layer thickness of 0.5 mm, showed 9.26 % higher tensile strength which indicated that the layer thickness has more significant impact on the strength. X. Tian et al. [47] reported maximum tensile strength and Young modulus of 256 MPa and 20.6 GPa, respectively with the 8.9 fiber volume content of CCF-PLA composites, while M. Heidari-Rarani et al. [22] reported tensile strength and Young modulus of 61.4 MPa and 8.28 GPa, respectively with the fiber volume content of 28.2. Other reported tensile strength of the PLA-CCF composites are 183 MPa [21], 91 MPa [39], 294.46 MPa [41] and 243.53 MPa [24].

The lowest Young's modulus value of 3.09 GPa was seen in the pure PLA specimen with the slightly increase up to 4.78 GPa in PLA-SF composite specimen. While, in the composite specimens printed with continuous fibers, G1 attained the highest Young's modulus value of 41.38 GPa, whereas the G4 with the layer thickness of 0.5 mm and line width of 1.2 mm reached the lowest modulus of 28.66 GPa among the composites specimens manufactured with CCF. G1 achieved 4 times and 2.5 times higher modulus in comparison to the tested PLA and PLA-SF specimens, respectively, and 44.3 % higher elasticity in contrast to G4 composite part. The results also proved that the lower the layer height and line width resulted in higher modulus and showed the consistency in the trend of the results with the tensile strengths. Moreover, the results evident that the higher content of the carbon fiber in the composites lead to higher Young's modulus [21,48,49] (see section 3.3). Table 3

Table 2
Parameters of the group samples.

Groups of samples	Group 1 (G1)	Group 2 (G2)	Group 3 (G3)	Group 4 (G4)
Layer thickness (mm)	0.4	0.5	0.4	0.5
Line width (mm)	1	1	1.2	1.2

To quantify the influence of printing parameters, Pearson correlation coefficients were calculated between layer thickness, line width, and tensile properties (Table 4). The results show a strong negative correlation between layer thickness and tensile strength ($r = -0.92$, $p < 0.01$) and Young's modulus ($r = -0.89$, $p < 0.01$), indicating that smaller layer thicknesses (0.4 mm) significantly enhance tensile properties. Line width showed a weaker negative correlation with tensile strength ($r = -0.65$, $p < 0.05$) and Young's modulus ($r = -0.62$, $p < 0.05$), suggesting a less pronounced effect. A two-way ANOVA (Table 5) confirmed that layer thickness has a statistically significant effect on tensile strength ($F(1,16) = 45.32$, $p < 0.001$) and Young's modulus ($F(1,16) = 38.76$, $p < 0.001$), with no significant interaction between layer thickness and line width ($p > 0.05$). Tukey's HSD test revealed that G1 significantly outperformed G2, G3, and G4 ($p < 0.05$), supporting the claim that layer thickness has a more significant impact on tensile properties.

3.1.2. Shear properties

The shear properties, specifically shear strength and shear modulus, of 3D-printed polymer composites incorporating CCF were evaluated through shear testing. The resulting shear stress-strain curves provide insight into the mechanical behavior of each CCF composite compared to commercial pure PLA and PLA-SF materials under shear loading, as shown in Fig. 7a. Each group exhibits unique mechanical characteristics, highlighting differences in elasticity, yield behavior, and strain-hardening capacity. The PLA sample demonstrated the lowest shear stress values, with an initial increase in stress reaching a relatively low peak at a low strain percentage, after which it stabilized. This behavior indicates a brittle nature with minimal plastic deformation, consistent with PLA's inherent rigidity and brittleness. PLA's lack of strain-hardening capability results in an early plateau in the stress-strain curve, underscoring its limited toughness. In contrast, the PLA-SF composite exhibited enhanced shear strength and greater strain tolerance compared to pure PLA. This improvement suggests that the carbon fibers contribute to more efficient load distribution and energy absorption within the PLA matrix, thereby enhancing the material's overall toughness [50]. Among the CCF composite groups, the G1 specimen achieved the highest shear stress, followed sequentially by G3, G2, and G4. G1 demonstrated the highest peak shear stress at a very low strain (~5 %), indicative of a highly rigid material with limited ductility. This sharp increase in stress with minimal strain suggests a composite capable of withstanding substantial force, though with limited deformation before failure. The G2 and G4 composites displayed a more gradual increase in shear stress with strain, achieving moderate peak values at relatively higher strain levels (approximately 15 % and 10 %, respectively). These curves suggest composites with moderate ductility and some strain-hardening ability, allowing them to endure more deformation before reaching peak stress, making them suitable for applications requiring a balance of strength and flexibility. The G3 composite demonstrated a rapid increase in shear stress, similar to G1, but reached a slightly lower peak. This initial rapid rise, followed by a peak, suggests that G3 possesses high shear strength but may experience a somewhat delayed failure compared to highly brittle materials.

The shear properties, shear strength and shear modulus, are presented in Fig. 7b and c, respectively. The results indicate that pure PLA exhibits the lowest shear strength at 9.07 MPa. In comparison, the PLA-SF composite achieves a shear strength of 23.39 MPa, representing an increase of 158 % over pure PLA. This improvement underscores the reinforcing effect of carbon fibers on the PLA matrix, significantly enhancing its load-bearing capacity. Among the CCF-reinforced composite specimens produced through 3D printing, the G1 sample, fabricated with a 0.4 mm layer thickness and 1 mm line width, achieved the highest shear strength at 33.89 MPa. This value surpasses that of other composite groups, with G2 and G3 attaining shear strengths of 24.72 MPa and 32.61 MPa, respectively, while G4 exhibited similar shear

Table 3
Mechanical properties measured from the experiments.

Specimens	Mechanical Properties					
	Tensile Properties		Shear Properties		Compression Properties	
	Tensile strength (MPa)	Young's modulus (GPa)	Shear strength (MPa)	Shear modulus (GPa)	Compression strength (MPa)	Compression modulus (GPa)
PLA	43.83 + 0.89	3.09 + 0.05	9.07 + 0.74	0.45 + 0.18	62.28 + 1.48	1.85 + 0.08
PLA-SF	44.08 + 1.02	4.78 + 0.08	23.39 + 1.38	0.51 + 0.24	60.59 + 1.23	2.47 + 0.14
G1	364.69 + 6.94	41.38 + 0.26	33.89 + 2.14	0.77 + 0.14	121.25 + 24.9	4.37 + 0.76
G2	287.48 + 8.80	29.60 + 0.29	25.03 + 1.20	0.54 + 0.09	98.41 + 18.75	3.17 + 0.37
G3	314.11 + 9.30	39.75 + 0.58	32.61 + 4.14	1.90 + 0.58	116.81 + 22.73	3.61 + 0.60
G4	242.87 + 8.39	28.66 + 0.42	24.20 + 2.88	2.38 + 0.33	101.89 + 25.77	3.39 + 0.58

Table 4
Pearson correlation coefficients for printing parameters and mechanical properties.

Parameter	Tensile Strength	Young's Modulus	Shear Strength	Shear Modulus	Compressive Strength	Compressive Modulus
Layer Thickness	−0.92**	−0.89**	−0.87**	−0.84**	−0.90**	−0.88**
Line Width	−0.65*	−0.62*	−0.60*	−0.58*	−0.63*	−0.61*

Note: **$p < 0.01$, *$p < 0.05$.

Table 5
Two-way ANOVA results for mechanical properties.

Property	Factor	F-Value	p-Value
Tensile Strength	Layer Thickness	45.32	<0.001
Tensile Strength	Line Width	12.67	<0.01
Tensile Strength	Interaction	1.23	0.29
Young's Modulus	Layer Thickness	38.76	<0.001
Young's Modulus	Line Width	10.45	<0.01
Young's Modulus	Interaction	0.98	0.34
Shear Strength	Layer Thickness	32.15	<0.001
Shear Strength	Line Width	9.88	<0.01
Shear Strength	Interaction	1.15	0.31
Shear Modulus	Layer Thickness	29.44	<0.001
Shear Modulus	Line Width	8.76	<0.05
Shear Modulus	Interaction	0.87	0.36
Compressive Strength	Layer Thickness	41.23	<0.001
Compressive Strength	Line Width	11.34	<0.01
Compressive Strength	Interaction	1.08	0.32
Compressive Modulus	Layer Thickness	37.89	<0.001
Compressive Modulus	Line Width	10.12	<0.01
Compressive Modulus	Interaction	0.95	0.35

strength to G2. Notably, G1 shear strength is 273.65 %, 45 %, 40 %, 37 %, and 4 % higher than that of PLA, PLA-SF, G2, G3, and G4, respectively, indicating the superior mechanical properties of this configuration. The PLA-SF and G4 composite materials displayed minimal variation in shear strength, with G4 showing only a modest 3.5 % increase compared to PLA-SF. These findings suggest that carbon fiber reinforcement, whether continuous or discontinuous, significantly enhances shear strength, while the influence of printing parameters, particularly layer thickness, is crucial in achieving optimal mechanical properties. A smaller layer thickness appears to yield a more compact composite structure, minimizing void volume (V_v) and contributing to the overall shear strength of the material [51].

The shear modulus results reveal distinct differences in the stiffness of the tested materials. The selected Pure PLA exhibited the lowest shear modulus at 0.45 GPa, with a slight increase to 0.51 GPa in the selected PLA-SF composite. However, within the CCF-reinforced composites, substantial variations were observed based on specific printing parameters. The G4 specimen, fabricated with a layer thickness of 0.5 mm and hatch spacing of 1.2 mm, achieved the highest shear modulus at 2.38 GPa, demonstrating a significant enhancement in stiffness. Conversely, the G2 specimen recorded the lowest shear modulus among the composites at 0.54 GPa. G1 and G3 reached shear modulus values of 0.77 GPa and 1.90 GPa, respectively. Notably, the G4 specimen exhibited increases of 209 %, 340 %, and 22 % in shear modulus compared to the G1, G2, and G3 composites, respectively. Additionally, when compared to pure PLA and PLA-SF, G4 displayed a shear modulus that was approximately 5.5 and 4.7 times higher, respectively, underscoring the impact of continuous carbon fiber reinforcement on stiffness. These findings indicate that greater layer thickness and hatch spacing contribute to increased flexibility and elasticity under shear loading conditions. However, while these parameters favor higher modulus values, optimal shear strength was observed with reduced layer thickness and line width, suggesting a trade-off between strength and flexibility in the design of CCF-reinforced composites. This balance of mechanical properties highlights the importance of tailored printing parameters to achieve specific performance characteristics in composite materials.

Correlation analysis (Table 4) revealed a strong negative correlation between layer thickness and shear strength ($r = -0.87$, $p < 0.01$) and shear modulus ($r = -0.84$, $p < 0.01$), with line width showing weaker correlations ($r = -0.60$, $p < 0.05$ for shear strength; $r = -0.58$, $p < 0.05$ for shear modulus). Two-way ANOVA (Table 5) indicated significant effects of layer thickness on shear strength ($F(1,16) = 32.15$, $p < 0.001$) and shear modulus ($F(1,16) = 29.44$, $p < 0.001$), with line width having a less significant effect ($p < 0.05$). Tukey's HSD test confirmed that G1's shear properties were significantly higher than those of G2, G3, and G4 ($p < 0.05$).

3.1.3. Compressive properties

A compression test was conducted to investigate the compressive properties specifically compressive strength and compressive modulus of 3D-printed polymer composites. The compressive stress-strain curves of the pure PLA, PLA-SF and composite groups are presented in Fig. 8a. These curves reveal that PLA-SF attains one of the lowest compressive stress levels, similar to pure PLA, with only a minimal increase. Among all tested materials, the highest average compressive stress was observed in G1, followed sequentially by G3, G4, and G2. PLA-SF showed limited compressive strength relative to the other materials tested. The PLA curve indicates a slightly higher compressive stress capacity than PLA-SF, with strain peaking around 2.5 %. This behavior aligns with PLA's brittle nature under compression, where it quickly reaches compressive strength without substantial strain-hardening, leading to an early plateau in the stress-strain curve. In contrast, G1 demonstrated the highest compressive stress of all groups, reaching peak stress at approximately 4 % strain. This steep rise in stress suggests that G1 is a highly rigid material with significant compressive strength. The subsequent slight drop after the peak indicates potential micro-cracking and localized failure within the composite structure. G2 exhibited a more gradual increase in compressive stress, peaking at a strain of about 4.5

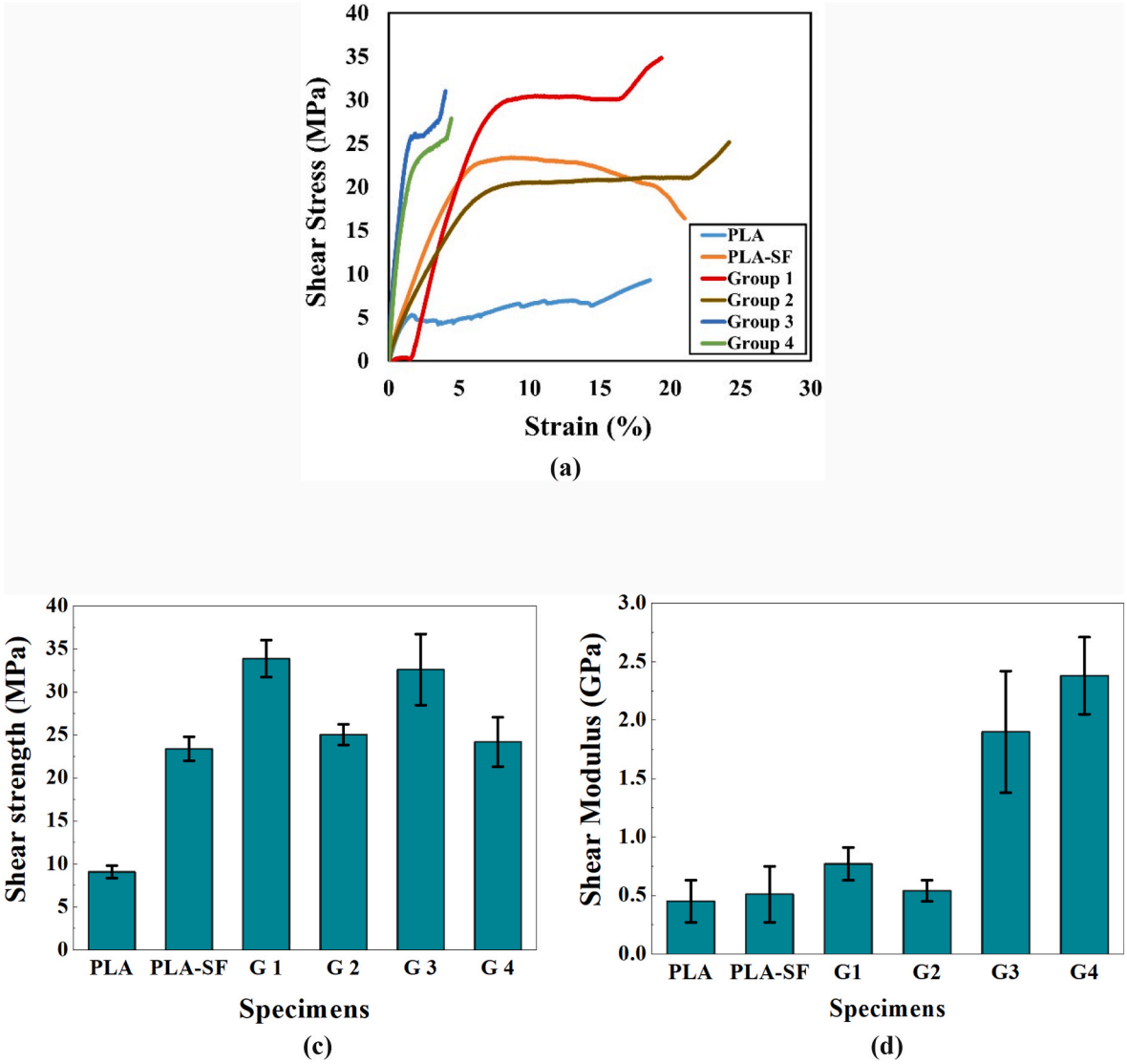

Fig. 7. Shear properties of the CCFRTC's groups fabricated material extrusion technique (a) shear stress-strain curves, (b) shear strength, (c) shear modulus.

%, reflecting moderate compressive strength and ductility with a stable response underloading. The absence of sharp stress drops after the peak suggests a uniform deformation behavior under compression, indicative of balanced stiffness and plasticity. G3 displayed a rapid increase in compressive stress, similar to G1, but achieved a slightly lower peak stress, suggesting it has a high compressive capacity with moderate plasticity. Meanwhile, G4 exhibited a distinctive curve, achieving peak compressive stress at around 5 % strain. This profile suggests that G4 not only possesses high compressive strength but also has enhanced strain tolerance compared to G1 and G3. The slight increase in stress beyond the initial peak implies strain-hardening behavior, enabling G4 to redistribute load effectively and resist further deformation under continued compressive stress.

The compressive properties, including compressive strength and compressive modulus, are presented in Fig. 8b and c, respectively. The results indicate that the lowest compressive strength, 60.59 MPa, was observed in the PLA-SF specimen, with a slight increase to 62.28 MPa in the pure PLA specimen. Among the polymer composite groups fabricated with CCF, the G1 specimen exhibited the highest compressive strength, reaching 121.25 MPa. This was followed by G3 and G4, with compressive strengths of 116.81 MPa and 101.89 MPa, respectively. The lowest compressive strength within the CCF groups, 98.41 MPa, was observed in G2, which was fabricated with a layer thickness of 0.5 mm and a line width of 1 mm, showing similar strength levels to G4. Notably, G1 demonstrated compressive strength nearly 95 % and 100 % higher than that of pure PLA and PLA-SF, respectively, and approximately 23 % higher than G2. These findings highlight that layer thickness plays a crucial role in determining the compressive strength of 3D-printed composite specimens. A thicker layer appears to enhance structural integrity, allowing for greater load-bearing capacity under compressive forces [51]. C. Zeng et al. [52] has reported maximum compressive strength compressive modulus of 72.1 MPa and 3.07 GPa, respectively with the fiber volume content of 13 % of PLA-CCF composite, while M. Araya-Calvo et al. [53] reported maximum compressive strength of 53.3 MPa and compressive modulus of 2.1 GPa with the fiber volume content of 24.44 % of PA6-CCF composite.

The lowest compressive modulus, 1.85 GPa, was observed in the pure PLA specimen. The incorporation of SFs into PLA significantly increased the compressive modulus of the PLA-SF specimen to 2.47 GPa, representing a 33.5 % improvement over pure PLA. Among the CCF-reinforced polymer composites, G1 achieved the highest compressive modulus at 4.37 GPa, while G2, G3, and G4 exhibited compressive moduli of 3.17 GPa, 3.61 GPa, and 3.39 GPa, respectively. G1 demonstrated a compressive modulus 2.4 times higher than pure PLA and 1.8 times higher than PLA-SF, and it also showed a 38 % increase in compressive modulus compared to G2. These results indicate that both

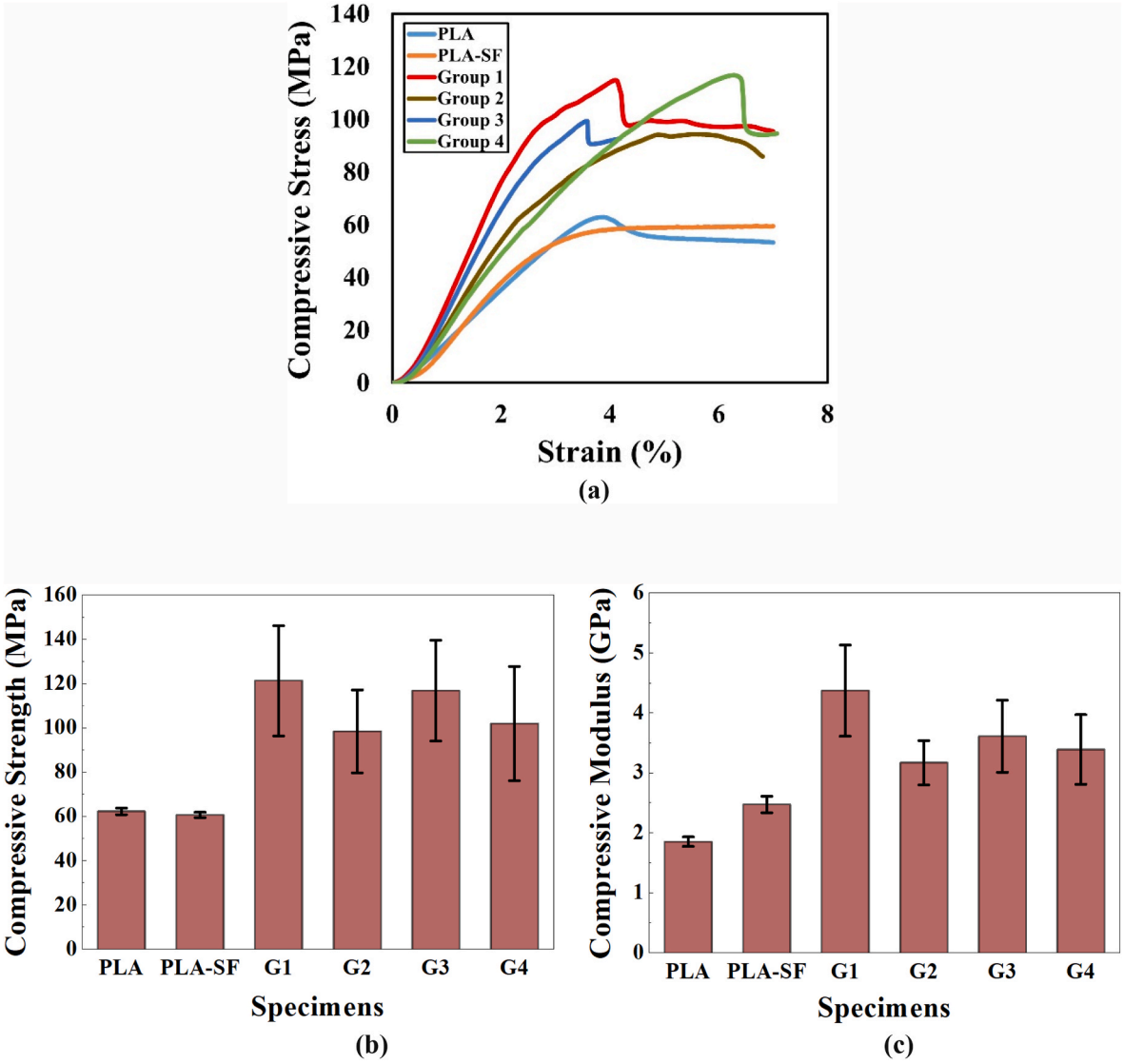

Fig. 8. Compressive properties of the CCFRTC's groups fabricated using FFF (a) compressive stress-strain curves, (b) compressive strength, (c) compressive modulus.

printing parameters and reinforcement content significantly impact the compressive modulus, leading to a more compact and robust structural formation. The addition of even small amounts of carbon fiber notably enhances the modulus, while increased fiber content contributes to both higher stiffness and flexibility. This highlights the importance of fiber reinforcement and optimized fabrication parameters in improving the compressive resistance of 3D-printed polymer composites.

Correlation analysis (Table 4) indicated strong negative correlations between layer thickness and compressive strength ($r = -0.90$, $p < 0.01$) and compressive modulus ($r = -0.88$, $p < 0.01$), with line width showing weaker correlations ($r = -0.63$, $p < 0.05$ for compressive strength; $r = -0.61$, $p < 0.05$ for compressive modulus). Two-way ANOVA (Table 5) confirmed significant effects of layer thickness on compressive strength ($F(1,16) = 41.23$, $p < 0.001$) and compressive modulus ($F(1,16) = 37.89$, $p < 0.001$), with no significant interaction effects ($p > 0.05$). Tukey's HSD test showed that G1's compressive properties were significantly higher than those of other groups ($p < 0.05$).

Table 3 presented the result of mechanical (tensile, shear and compressive) properties measured from the experiments.

3.2. X-ray micro-CT scan result analysis

The CT scan images of the 3D-printed polymer structure provide valuable insights into key internal features, including layer formation, void distribution, potential delamination zones, and density variations. These characteristics are pivotal in determining the porosity and structural performance of additively manufactured parts. Analyzing and understanding these particulars facilitates the optimization of printing parameters to enhance the strength, reliability, and overall quality of 3D-printed components.

X-ray micro-CT scanning was employed to examine the internal structure and determine the porosity and internal voids of 3D-printed CCFRTC with varied layer thicknesses and line widths. The CT images of each composite group, shown in Fig. 9, reveal a complex arrangement of interconnected layers that represent the sequential material deposition during the 3D printing process. Notably, the presence of porosity was observed across all composite groups, with voids being particularly evident. The analysis showed that increasing the layer thickness and line width led to higher porosity levels. G1, characterized by the smallest layer thickness and line width, exhibited the lowest porosity, correlating with a higher density due to a more substantial amount of deposited carbon fibers.

The formation of voids in 3D-printed composites can result from

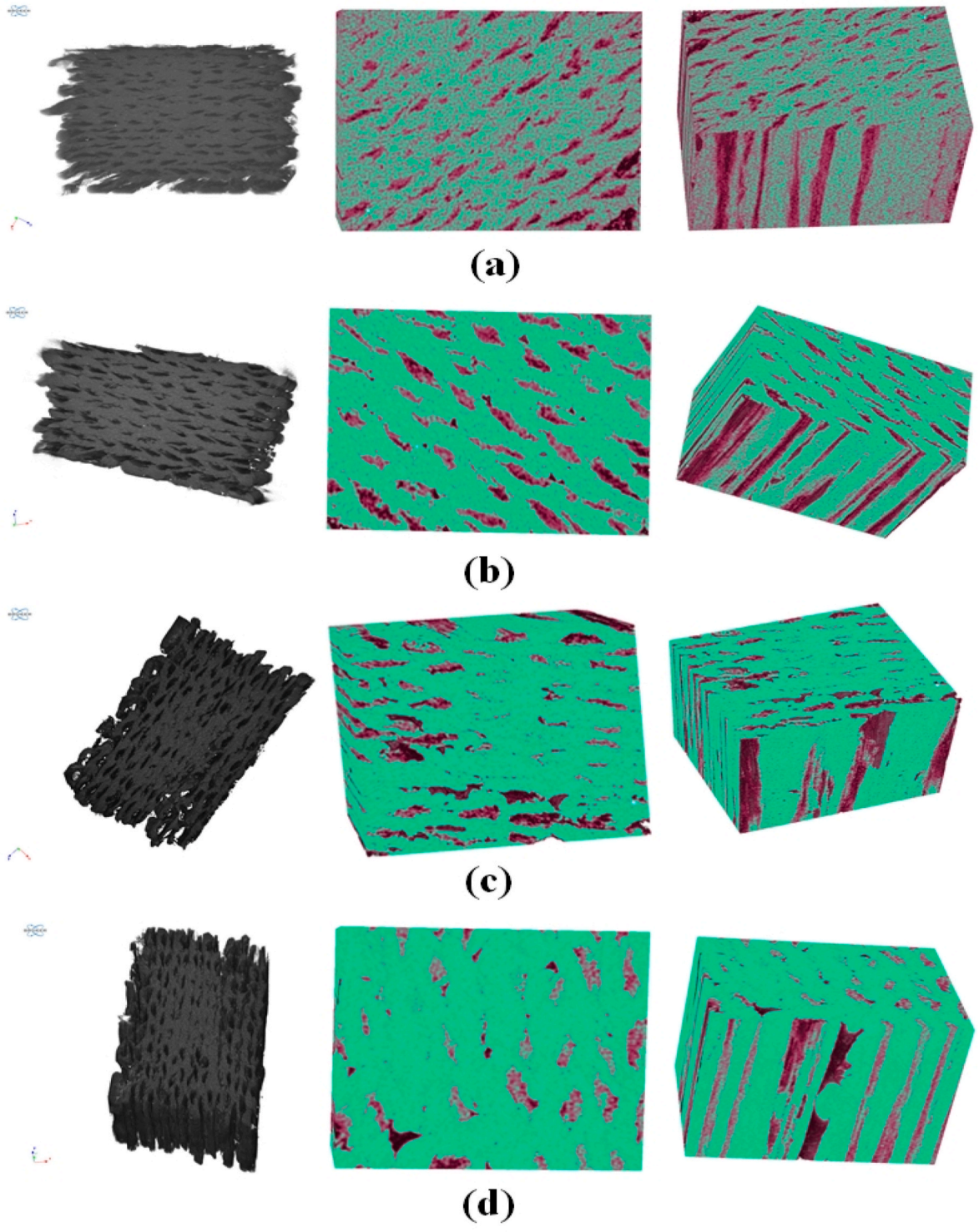

Fig. 9. X-ray micro-CT scan images of the polymer composites a) G1, b) G2, c) G3 and d) G4.

incomplete layer adhesion, under-extrusion, or entrapped air during the printing process. These voids act as stress concentrators, which can severely compromise the mechanical integrity of the structure by reducing its overall strength and durability. In particular, the CT image of the G2 and G4 specimens displayed distinct layer boundaries, indicative of higher porosity levels and the presence of voids compared to other composite groups. This observation aligns with mechanical testing results, which showed that G4 exhibited the lowest strength among all tested composite groups.

To obtain an average porosity value, three samples from each group were analyzed. The CT scan results indicated that G1 had the lowest porosity at 16.14 % ± 0.58, while G2, G3, and G4 exhibited average porosities of 21.96 % ± 0.91, 19.91 % ± 1.64, and 21.33 % ± 1.27, respectively. The porosity levels of G2 and G4 were nearly identical, showing no significant differences. Fig. 10 presents the porosity content measured in each polymer composite group using X-ray CT scanning.

The data demonstrated that porosity levels decreased with a reduction in layer thickness and line width. Lowering the layers thickness and line widths resulted in more compact structures with reduced spacing between layers, promoting better bonding and fewer voids. This

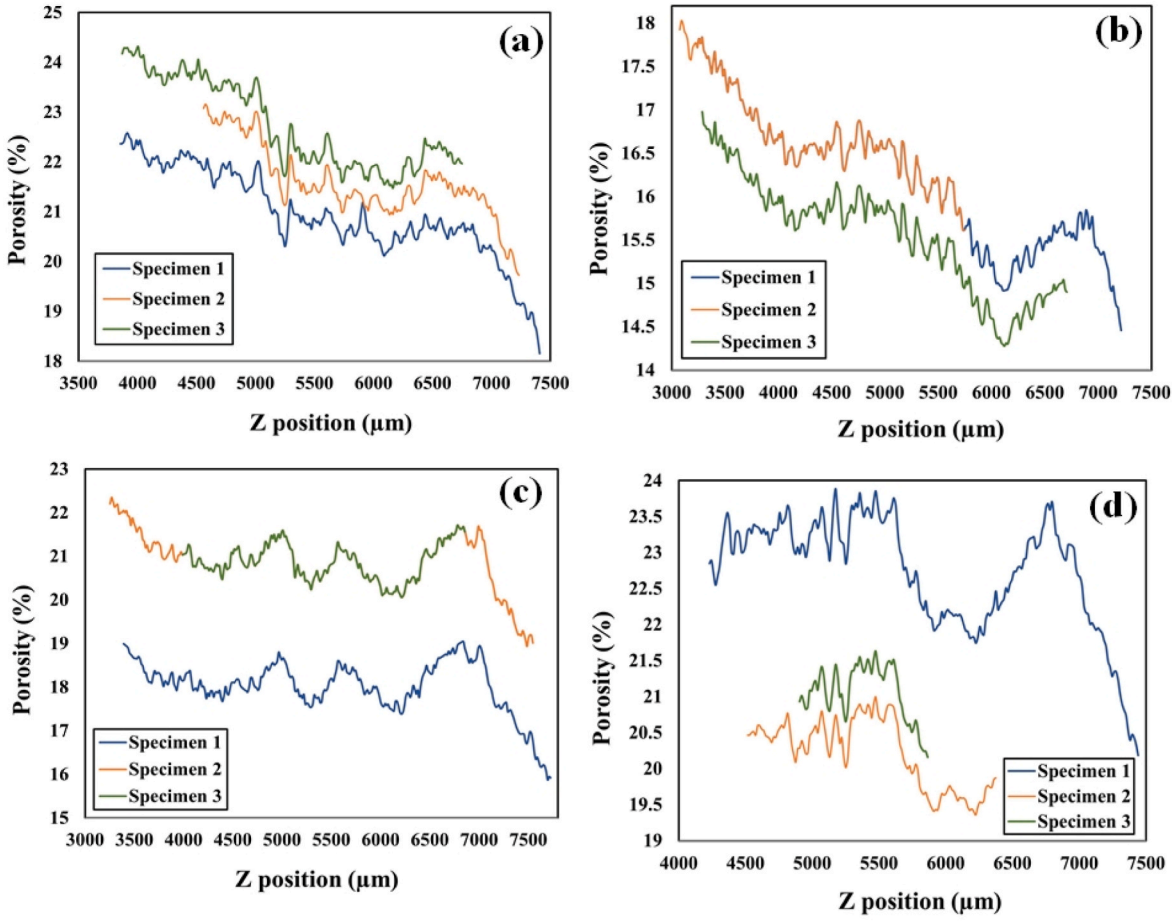

Fig. 10. Porosity measured in the composite specimens using X-ray CT scan a) G1, b) G2, c) G3, d) G4.

improved layer contact minimizes void formation, which correlates with better mechanical performance. Although the minimum porosity achieved was 16.14 %, which compares favorably with similar PLA-CCF studies, further reduction is necessary to meet the standards of structural applications. However, the enhanced impregnation techniques and post-processing infiltration, dynamic pressure-assisted printing, and real-time thermal control to improve polymer flow and minimize void formation.

The mechanical testing results corroborated the porosity findings, as G1, with the lowest porosity, exhibited superior mechanical properties compared to the other groups. This relationship emphasizes the critical influence of printing parameters on the internal structure and porosity of 3D-printed polymer composites. These results underscore the need for precise control of fabrication conditions to minimize defects, optimize porosity levels, and enhance the performance of 3D-printed components.

The porosity trends along the Z-axis further explain the differences. G1 and G2 with 1.0 mm line width show a declining porosity trend, indicating improved consolidation in upper layers, which enhances mechanical performance. G3 and G4 with 1.2 mm line width exhibit uniform or scattered porosity, suggesting inconsistent fusion due to increased material deposition, which weakens mechanical properties.

Table 6 shows the porosity measured from the CT scan results for the continuous fiber composites.

The incorporation of a directed cooling fan system in the custom-built 3D printer allowed better control of polymer solidification dynamics, especially in samples with lower layer thickness. This facilitated more consistent layer deposition and minimized sagging or thermal distortion. However, excessive cooling in certain geometries may have hindered interlayer diffusion, possibly contributing to observed interfacial voids in micro-CT. Thus, the cooling system played a dual role enhancing geometric precision while occasionally limiting polymer chain entanglement across layers.

Table 6
Average porosity calculated from CT scan for each composite's group.

Composite group	Specimen	Porosity (%)	Average porosity (%)
G1	Specimen 1	16.16	16.14
	Specimen 2	16.71	
	Specimen 3	15.55	
G2	Specimen 1	20.96	21.96
	Specimen 2	22.17	
	Specimen 3	22.74	
G3	Specimen 1	18.01	19.91
	Specimen 2	20.86	
	Specimen 3	20.86	
G4	Specimen 1	22.73	21.33
	Specimen 2	20.22	
	Specimen 3	21.06	

3.3. Fiber volume fraction of composites

The results revealed that G1 exhibited the highest V_f, reaching 26.12 %, followed by G3 with 23.84 %, G2 with 21.53 %, and G4 with the lowest V_f of 18.87 %. These findings correlate strongly with the mechanical properties of the composites, as specimens with higher V_f demonstrated superior mechanical performance. This relationship underscores the critical role of reinforcement content in determining the mechanical strengths and elastic modulus of fiber-reinforced

composites. The higher V_f enhances the load-bearing capacity and stiffness of the composite by increasing the contribution of the high-strength carbon fibers to the overall mechanical behavior [54,55].

Furthermore, the results indicate that layer thickness significantly influences the reinforcement content. Specimens fabricated with smaller layer thicknesses exhibited higher V_f values due to reduced interlayer voids and improved fiber packing density. These results are consistent with the mechanical testing, where composites with the highest V_f (G1) displayed the best performance in terms of strength and modulus, while lower reinforcement content (G4) was associated with reduced mechanical properties.

Fig. 11a illustrates the measured reinforcement content of CCF within the additively manufactured composite specimens as determined by the dissolution method. The findings emphasize the importance of precise control over printing parameters to achieve optimal fiber content and, consequently, enhanced mechanical properties in 3D-printed composites. A linear regression was applied to evaluate the relationship between V_f and tensile strength (Fig. 11b). The resulting coefficient of determination ($R^2 = 0.987$) indicates a strong linear correlation, suggesting that the increase in fiber content positively influences tensile strength in an approximately proportional manner. However, deviations at higher V_f levels may arise due to local porosity or fiber misalignment, which are not accounted for in the linear model.

3.4. Scanning electron microscopy analysis

Fig. 12 shows SEM images of the fractured region of the specimen of each composite group after the tensile loading fracture. Each group of 3D printed polymer composite showed similar behavior of fracture mode after the tensile loading.

The fracture observed in the polymer composite specimens exhibits characteristics indicative of a predominantly brittle failure mode. This is evident from the relatively smooth fracture surface with minimal signs of plastic deformation. The elongated carbon fibers visible in the fractured area suggest that they were well-aligned during the composite manufacturing process, enhancing the material's tensile strength along the direction of fiber orientation.

In certain sections, fiber pullout is observed, leaving behind voids or cavities. This occurrence is typical in fiber-reinforced composites where the fiber-matrix interface bond is insufficient [56]. Such pullout points to a failure in adhesion, often a critical factor when the bond strength between the fibers and matrix is weaker than the tensile strength of the fibers themselves. This interfacial weakness can be attributed to suboptimal surface treatment of fibers or insufficient infiltration of the matrix during processing. The matrix material, PLA, exhibits visible cracks and fissures, which are likely initiated at the fiber-matrix interfaces due to stress concentrations. These cracks propagated through the matrix, indicative of rapid crack growth characteristic of brittle fracture. The occurrence of fibers fractured within the matrix suggests that, in some instances, the fibers reached their ultimate tensile strength before the interface bond failed, underscoring effective load transfer within the composite. The absence of significant plastic deformation implies that the fracture propagated swiftly through the composite, without significant energy absorption (Fig. 12a).

The SEM image (Fig. 12b) highlights a region where the CCF remains integrated within the matrix, alongside areas showing void formation. The intact CCF within the matrix demonstrates effective adhesion in certain regions, indicating that the load transfer between fibers and the PLA matrix was successful up to a certain point. However, the void formation suggests processing defects or stress-induced de-bonding during tensile loading. The CCF remained intact within the matrix. This indicates that the fiber-matrix interface was strong enough to withstand the applied stress. Fiber pullout occurs when the interfacial bond between the fiber and the matrix is weaker than the fiber itself. This can be attributed to various factors, including poor adhesion, improper surface treatment of the fibers, or insufficient matrix infiltration during the manufacturing process [57,58].

G1's strong fiber-matrix adhesion and minimal voids result from optimized layer thickness (0.4 mm) and line width (1.0 mm), promoting effective load transfer and high mechanical performance. G2's increased voids and moderate fiber pull-out reflect the negative impact of thicker layers (0.5 mm), which reduce interlayer bonding and increase porosity. G3's fiber pull-out and matrix cracking indicate that the wider line width (1.2 mm) introduces defects, despite the benefits of thinner layers (0.4 mm). G4's poor adhesion and matrix-dominated failure highlight the combined detrimental effects of thicker layers and wider line width, leading to high porosity and reduced mechanical integrity.

3.5. ROM model for the prediction of elastic modulus and tensile strength

The results reveal a consistent trend between the experimental data and the predictions obtained using the ROM. As shown in Fig. 13a and b, highlighting the correlation between experimental and theoretical values for Young's modulus and tensile strength are consistently lower than the theoretical predictions from the ROM. However, the influence of printing parameters, such as layer height and line width, is evident in the experimental results, confirming their significant impact on the tensile properties of the composites. Both the experimental and theoretical results demonstrate that an increase in fiber content substantially enhances the tensile strength and elastic modulus of the composite

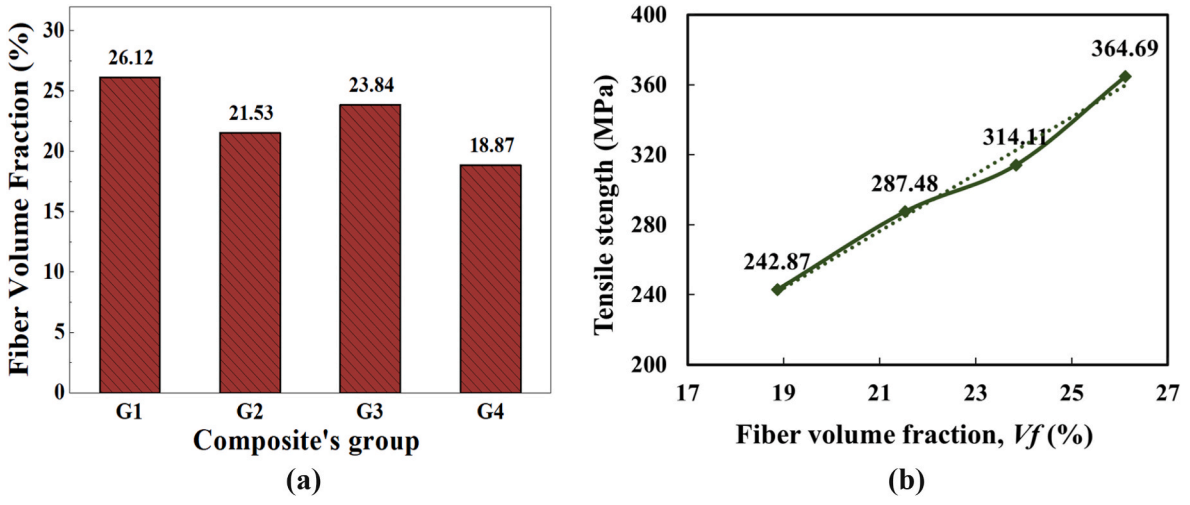

Fig. 11. (a) Carbon fiber content measured in composite groups using dissolution procedure, (b) linear correlation between the fiber content and tensile strength.

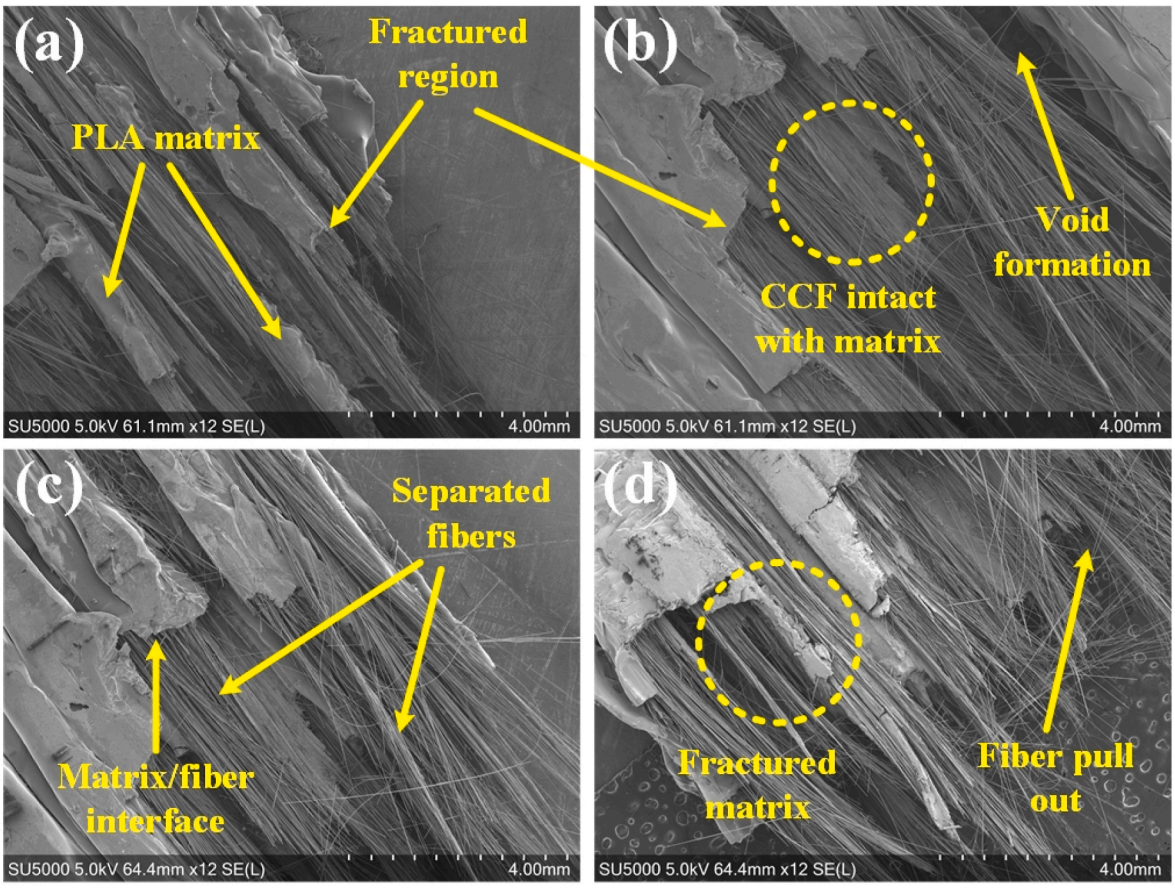

Fig. 12. SEM micrographs of fractured composite specimens of a) G1; b) G2; c) G3; d) G4, after performing tensile test.

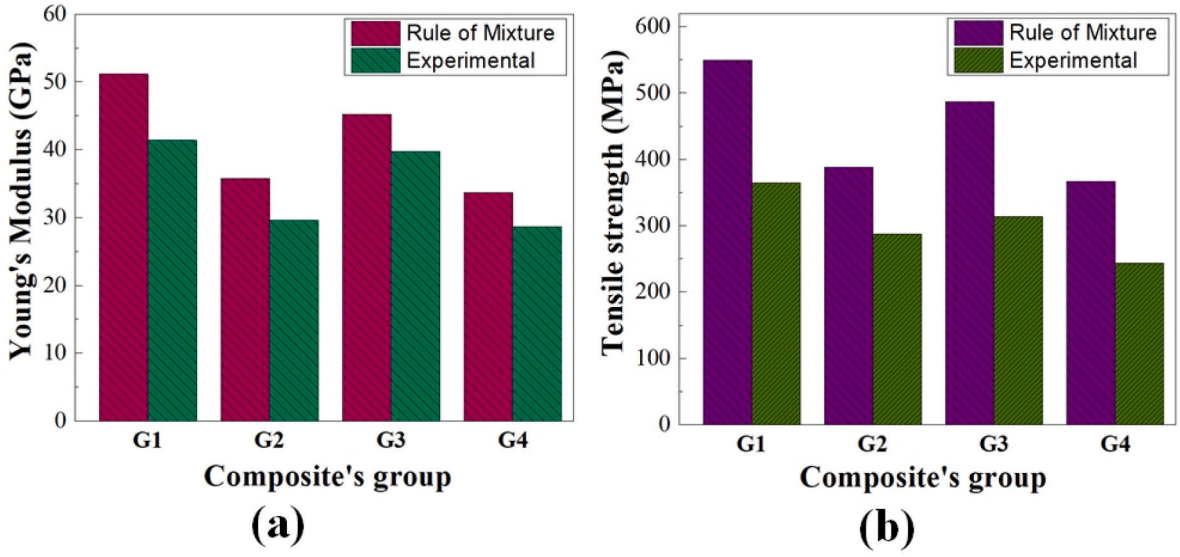

Fig. 13. Predicted results calculated using ROM; (a) theoretical and experimental elastic modulus, (b) theoretical and experimental tensile strength.

specimens. While the ROM-predicted Young's modulus closely aligns with the experimental results, the tensile strength predictions exhibit a notable deviation. Table 7 summarizes the predicted E_c and X_c values calculated using the ROM. This comparison demonstrates the utility of the ROM in establishing baseline theoretical values, which can be used to evaluate the impact of manufacturing parameters and material properties on the performance of 3D-printed composites.

Even after accounting for void volume V_v in the ROM, the predicted values for the elastic modulus E_c and tensile strength X_c remain lower than those observed in composites produced under ideal conditions. This discrepancy arises from multiple factors. First, the 3D printing process inherently involves bonding challenges, such as weak interlayer adhesion and incomplete fusion between deposited lines, which introduce structural imperfections. Additionally, issues at the fiber-matrix

Table 7
Predicted Young's modulus (E_c) and tensile strength (X_c) using ROM with Goodness of Fit.

Composite's group	Predicted Young's modulus (E_c)	Experimental Young's modulus	Predicted Tensile strength (X_c)	Experimental Tensile strength
G1	51.13 GPa	41.38 GPa	549.30 MPa	364.69 MPa
G2	35.76 GPa	29.60 GPa	387.97 MPa	287.48 MPa
G3	45.18 GPa	39.75 GPa	486.60 MPa	314.11 MPa
G4	33.66 GPa	28.66 GPa	366.19 MPa	242.87 MPa
Goodness of Fit	**R^2 = 0.97**	**RMSE = 5.76 GPa**	**R^2 = 0.58**	**RMSE = 149.07 MPa**

interface further impact load transfer efficiency, contributing to reduced mechanical performance. Second, experimental testing introduces variables that can deviate from ideal conditions. Factors such as specimen gripping during tensile tests, alignment inconsistencies, and variations in environmental conditions (e.g., temperature and humidity) can significantly influence the measured mechanical properties.

While the ROM model offers a first-order approximation of tensile modulus and strength based on volume fractions and constituent properties, it relies on idealized assumptions, including perfect load transfer, flawless fiber alignment, and complete interfacial bonding. However, practical deviations arise due to several key factors: 1. Fiber–matrix interfacial bonding – Imperfect adhesion between the fiber and matrix reduces load transfer efficiency. SEM images (Fig. 12) reveal signs of interfacial debonding and incomplete matrix infiltration. 2. Fiber orientation dispersion – The ROM assumes perfect fiber alignment along the loading direction, but in practice, factors such as deposition path curvature and nozzle vibration lead to local misalignments. 3. Void content and defects – Despite reduced porosity (16.1 %), voids near fiber interfaces interrupt stress transfer pathways and compromise mechanical strength. CT and SEM analyses identified both micro- and macro-voids that are not accounted for in ROM predictions. 4. Matrix plasticity and failure behavior – The PLA matrix exhibits brittle fracture under tensile loading, whereas the ROM model assumes linear-elastic behavior, neglecting the effects of stress concentrations and premature matrix cracking.

In contrast, the ROM assumes an idealized scenario, focusing solely on the effect of void volume while neglecting other critical variables. This model does not account for factors like interface quality, manufacturing inconsistencies, and testing anomalies, all of which play a significant role in determining the actual performance of the composite. For future work, enhancing the ROM by incorporating additional variables and refining assumptions could improve its alignment with experimental results, offering a more comprehensive predictive tool for composite materials.

The goodness-of-fit analysis quantifies the agreement between experimental and ROM-predicted values. For Young's modulus, the high R^2 value (0.97) and relatively low RMSE (5.76 GPa) indicate strong agreement, suggesting that the ROM accurately predicts composite stiffness. The largest deviation is for G1 (41.38 GPa experimental vs. 51.13 GPa predicted, 23.6 % error), but the overall trend across groups aligns closely with ROM predictions, with deviations ranging from 14.2 % (G4) to 23.6 % (G1). This accuracy reflects the ROM's reliance on V_f and linear elastic behavior, which are well-characterized.

For tensile strength, the lower R^2 value (0.58) and high RMSE (149.07 MPa) indicate significant deviations, with ROM overestimating experimental values. G1's experimental tensile strength (364.69 MPa) is 66.4 % of the predicted value (549.30 MPa), and G4 shows the largest deviation (242.87 MPa vs. 366.19 MPa, 66.3 %). These discrepancies are attributed to processing-induced defects, such as voids and poor fiber-matrix adhesion, which reduce load transfer and are not accounted for in the ROM [48].

These findings emphasize the importance of optimizing printing parameters and minimizing defects during fabrication to bridge the gap between theoretical predictions and experimental performance, ensuring improved mechanical properties in 3D-printed continuous fiber-reinforced composites [59].

4. Conclusion

This experimental study investigated the manufacturing of CCFRTCs using an in-situ co-extrusion technique with towpreg material extrusion, incorporating external controlled cooling. The research emphasized the critical influence of printing process parameters, specifically layer thickness and line width, on the tensile, shear, and compressive properties, as well as porosity and V_f of the FFF-printed polymer composites. Composite groups were fabricated with varying layer thicknesses and line widths, and their performance was compared to baseline specimens made of pure PLA and PLA-SF. The results demonstrate that the CCFRTCs manufactured with a layer thickness of 0.4 mm and line width of 1 mm (G1) achieved the highest tensile, shear, and compressive strengths, measured at 364.69 MPa, 33.89 MPa, and 121.25 MPa, respectively. These values represent substantial increases of 732 %, 340 %, and 94.6 %, respectively, compared to the baseline materials. Additionally, G1 exhibited the highest V_f of 26.12 %, as determined using the dissolution method, and the lowest porosity of 16.14 %, quantified via X-ray micro-CT analysis. These findings confirm that reducing layer thickness and line width results in a more compact and well-bonded structure, characterized by improved interlayer adhesion, higher fiber content, and reduced porosity. Such structural improvements significantly enhance the mechanical performance of the composites under tensile, shear, and compressive loadings. Furthermore, this research provides detailed insights into the interplay between printing parameters, structural integrity, and mechanical properties, guiding future optimizations to improve the performance and quality of 3D-printed thermoplastic composites. The customized cooling system introduced in this study helped achieve better dimensional control and surface finish, particularly at thinner layer heights. However, its influence on interlayer bonding strength appears to be parameter-sensitive and may need further optimization depending on print speed and thermal diffusion requirements. The outcomes of this study highlight the potential for tailored manufacturing strategies to achieve high-performance, fiber-reinforced polymer composites for advanced applications.

CRediT authorship contribution statement

Nabeel Maqsood: Writing – original draft, Visualization, Validation, Methodology, Investigation, Funding acquisition, Formal analysis, Data curation, Conceptualization. **Jawad Ullah:** Writing – review & editing, Visualization, Validation, Resources, Methodology, Investigation, Formal analysis, Data curation. **Marius Rimašauskas:** Writing – review & editing, Visualization, Validation, Supervision, Resources, Investigation, Formal analysis, Conceptualization. **Kateřina Skotnicová:** Writing – review & editing, Visualization, Validation, Resources, Project administration, Investigation, Funding acquisition, Formal analysis. **Genrik Mordas:** Writing – review & editing, Visualization, Validation, Resources, Methodology, Investigation, Formal analysis, Data curation. **Conor McCrickard:** Visualization, Software, Resources, Methodology, Investigation, Formal analysis, Data curation. **Joamin Gonzalez-Gutierrez:** Writing – review & editing, Visualization, Validation, Resources, Methodology, Investigation, Formal analysis. **Alistair McIlhagger:** Visualization, Validation, Resources, Investigation. **Edward Archer:** Visualization, Validation, Resources.

Declaration of competing interest

The authors declare that they have no known competing financial

interests or personal relationships that could have appeared to influence the work reported in this paper.

Acknowledgement

This article has been produced with the financial support of the European Union under the REFRESH – Research Excellence For REgion Sustainability and High-tech Industries project number CZ.10.03.01/00/22_003/0000048 via the Operational Programme Just Transition.

References

[1] P. Parandoush, D. Lin, A review on additive manufacturing of polymer-fiber composites, Compos. Struct. 182 (2017) 36–53, https://doi.org/10.1016/j.compstruct.2017.08.088.
[2] N. Maqsood, M. Rimasauskas, A review on development and manufacturing of polymer matrix composites using 3D printing technologies, in: 9th International Scientific Conference on Defensive Technologies - OTEH, 2020, pp. 462–468.
[3] F. Ning, W. Cong, Y. Hu, H. Wang, Additive manufacturing of carbon fiber-reinforced plastic composites using fused deposition modeling: effects of process parameters on tensile properties, J. Compos. Mater. 51 (2017) 451–462, https://doi.org/10.1177/0021998316646169.
[4] N. Maqsood, M. Rimašauskas, Delamination observation occurred during the flexural bending in additively manufactured PLA-Short carbon fiber filament reinforced with continuous carbon fiber composite, Results Eng. 11 (2021) 100246, https://doi.org/10.1016/j.rineng.2021.100246.
[5] A.N. Dickson, J.N. Barry, K.A. McDonnell, D.P. Dowling, Fabrication of continuous carbon, glass and kevlar fibre reinforced polymer composites using additive manufacturing, Addit. Manuf. 16 (2017) 146–152, https://doi.org/10.1016/j.addma.2017.06.004.
[6] M. Rimašauskas, T. Kuncius, R. Rimašauskienė, Processing of carbon fiber for 3D printed continuous composite structures, Mater. Manuf. Process. 34 (2019) 1528–1536, https://doi.org/10.1080/10426914.2019.1655152.
[7] A. El Moumen, M. Tarfaoui, K. Lafdi, Additive manufacturing of polymer composites: processing and modeling approaches, Compos. B Eng. 171 (2019) 166–182, https://doi.org/10.1016/j.compositesb.2019.04.029.
[8] A.D. Valino, J.R.C. Dizon, A.H. Espera, Q. Chen, J. Messman, R.C. Advincula, Advances in 3D printing of thermoplastic polymer composites and nanocomposites, Prog. Polym. Sci. 98 (2019) 101162, https://doi.org/10.1016/j.progpolymsci.2019.101162.
[9] T. Yu, Z. Zhang, S. Song, Y. Bai, D. Wu, Tensile and flexural behaviors of additively manufactured continuous carbon fiber-reinforced polymer composites, Compos. Struct. 225 (2019) 111147, https://doi.org/10.1016/j.compstruct.2019.111147.
[10] N. Maqsood, M. Rimašauskas, M. Ghobakhloo, G. Mordas, K. Skotnicová, Additive manufacturing of continuous carbon fiber reinforced polymer composites using materials extrusion process. Mechanical properties, process parameters, fracture analysis, challenges, and future prospect. A review, Adv. Compos. Hybrid Mater. 7 (2024) 202, https://doi.org/10.1007/s42114-024-01035-w.
[11] J.M. Chacón, M.A. Caminero, P.J. Núñez, E. García-Plaza, I. García-Moreno, J. M. Reverte, Additive manufacturing of continuous fibre reinforced thermoplastic composites using fused deposition modelling: effect of process parameters on mechanical properties, Compos. Sci. Technol. 181 (2019) 107688, https://doi.org/10.1016/j.compscitech.2019.107688.
[12] P. Zhuo, S. Li, I.A. Ashcroft, A.I. Jones, Continuous fibre composite 3D printing with pultruded carbon/PA6 commingled fibres: processing and mechanical properties, Compos. Sci. Technol. 221 (2022) 109341, https://doi.org/10.1016/j.compscitech.2022.109341.
[13] X. Wang, M. Jiang, Z. Zhou, J. Gou, D. Hui, 3D printing of polymer matrix composites: a review and prospective, Compos. B Eng. 110 (2017) 442–458, https://doi.org/10.1016/j.compositesb.2016.11.034.
[14] H.A. Hegab, Design for additive manufacturing of composite materials and potential alloys: a review, Manuf. Rev. 3 (2016) 1–17, https://doi.org/10.1051/mfreview/2016010.
[15] N. Maqsood, M. Rimašauskas, Tensile and flexural response of 3D printed solid and porous CCFRPC structures and fracture interface study using image processing technique, J. Mater. Res. Technol. 14 (2021) 731–742, https://doi.org/10.1016/j.jmrt.2021.06.095.
[16] Y. Wu, K. Wang, V. Neto, Y. Peng, R. Valente, S. Ahzi, Interfacial behaviors of continuous carbon fiber reinforced polymers manufactured by fused filament fabrication : a review and prospect, Int. J. Material Form. (2023), https://doi.org/10.1007/s12289-022-01667-7.
[17] Z. Xin, Y. Ma, Y. Chen, B. Wang, H. Xiao, Y. Duan, Fusion-bonding performance of short and continuous carbon fiber synergistic reinforced composites using fused filament fabrication, Composites, Part B 248 (2023) 110370, https://doi.org/10.1016/j.compositesb.2022.110370.
[18] J.T. Green, I.A. Rybak, J.J. Slager, M. Lopez, Z. Chanoi, C.M. Stewart, R. V. Gonzalez, Local composition control using an active-mixing hotend in fused filament fabrication, Additive Manufacturing Letters 7 (2023) 100177, https://doi.org/10.1016/j.addlet.2023.100177.
[19] A. Matschinski, Integration of continuous fibers in additive manufacturing processes, in: Virtual Symposium on AFP and AM, Technical University of Munich and Australian National University, 2020.
[20] F. Wang, G. Wang, H. Wang, R. Fu, Y. Lei, J. He, 3D printing technology for short-continuous carbon fiber synchronous reinforced thermoplastic composites: a comparison between towpreg extrusion and in situ impregnation processes, Chin. J. Mech. Eng.: Additive Manufacturing Frontiers 2 (2023) 100092, https://doi.org/10.1016/j.cjmeam.2023.100092.
[21] M. Rimašauskas, E. Jasiūnienė, T. Kuncius, R. Rimašauskienė, V. Cicėnas, Investigation of influence of printing parameters on the quality of 3D printed composite structures, Compos. Struct. 281 (2022) 115061, https://doi.org/10.1016/j.compstruct.2021.115061.
[22] M. Heidari-Rarani, M. Rafiee-Afarani, A.M. Zahedi, Mechanical characterization of FDM 3D printing of continuous carbon fiber reinforced PLA composites, Compos. B Eng. 175 (2019) 107147, https://doi.org/10.1016/j.compositesb.2019.107147.
[23] R. Matsuzaki, M. Ueda, M. Namiki, T.-K. Jeong, H. Asahara, K. Horiguchi, T. Nakamura, A. Todoroki, Y. Hirano, Three-dimensional printing of continuous-fiber composites by in-nozzle impregnation, Sci. Rep. 6 (2016) 23058, https://doi.org/10.1038/srep23058.
[24] H. Dou, Y. Cheng, W. Ye, D. Zhang, J. Li, Z. Miao, S. Rudykh, Effect of process parameters on tensile mechanical properties of 3D printing continuous carbon fiber-reinforced PLA composites, Materials 13 (2020), https://doi.org/10.3390/ma13173850.
[25] H. Zhang, J. Wang, Y. Liu, X. Zhang, Z. Zhao, Effect of processing parameters on the printing quality of 3D printed composite cement-based materials, Mater. Lett. 308 (2022) 131271, https://doi.org/10.1016/j.matlet.2021.131271.
[26] Y.Y. Aw, C.K. Yeoh, M.A. Idris, P.L. Teh, K.A. Hamzah, S.A. Sazali, Effect of printing parameters on tensile, dynamic mechanical, and thermoelectric properties of FDM 3D printed CABS/znO composites, Materials 11 (2018), https://doi.org/10.3390/ma11040466.
[27] C. Yang, X. Tian, T. Liu, Y. Cao, D. Li, 3D printing for continuous fiber reinforced thermoplastic composites: mechanism and performance, Rapid Prototyp. J. 23 (2017) 209–215, https://doi.org/10.1108/RPJ-08-2015-0098.
[28] M. Moradi, M.K. Moghadam, M. Shamsborhan, M. Bodaghi, The synergic effects of fdm 3d printing parameters on mechanical behaviors of bronze poly lactic acid composites, Journal of Composites Science 4 (2020) 1–16, https://doi.org/10.3390/jcs4010017.
[29] A. Pentek, M. Nyitrai, A. Schiffer, H. Abraham, M. Bene, E. Molnar, R. Told, P. Maroti, The effect of printing parameters on electrical conductivity and mechanical properties of PLA and ABS based carbon composites in additive manufacturing of upper limb prosthetics, Crystals 10 (2020) 1–12, https://doi.org/10.3390/cryst10050398.
[30] K.G.J. Christiyan, U. Chandrasekhar, K. Venkateswarlu, A study on the influence of process parameters on the mechanical properties of 3D printed ABS composite, IOP Conf. Ser. Mater. Sci. Eng. (2016) 114, https://doi.org/10.1088/1757-899X/114/1/012109.
[31] M. Nabipour, B. Akhoundi, An experimental study of FDM parameters effects on tensile strength, density, and production time of ABS/Cu composites, J. Elastomers Plast. 53 (2021) 146–164, https://doi.org/10.1177/0095244320916838.
[32] D. Godec, S. Cano, C. Holzer, J. Gonzalez-Gutierrez, Optimization of the 3D printing parameters for tensile properties of specimens produced by fused filament fabrication of 17-4PH stainless steel, Materials 13 (2020), https://doi.org/10.3390/ma13030774.
[33] F. Ning, W. Cong, J. Qiu, J. Wei, S. Wang, Additive manufacturing of carbon fiber reinforced thermoplastic composites using fused deposition modeling, Compos. B Eng. 80 (2015) 369–378, https://doi.org/10.1016/j.compositesb.2015.06.013.
[34] P. Bettini, G. Alitta, G. Sala, L. Di Landro, Fused deposition technique for continuous fiber reinforced thermoplastic, J. Mater. Eng. Perform. 26 (2017) 843–848, https://doi.org/10.1007/s11665-016-2459-8.
[35] T.D. Ngo, A. Kashani, G. Imbalzano, K.T.Q. Nguyen, D. Hui, Additive manufacturing (3D printing): a review of materials, methods, applications and challenges, Compos. B Eng. 143 (2018) 172–196, https://doi.org/10.1016/j.compositesb.2018.02.012.
[36] M.A. Gibson, N.M. Mykulowycz, J. Shim, R. Fontana, P. Schmitt, A. Roberts, J. Ketkaew, L. Shao, W. Chen, P. Bordeenithikasem, J.S. Myerberg, R. Fulop, M. D. Verminski, E.M. Sachs, Y.M. Chiang, C.A. Schuh, A. John Hart, J. Schroers, 3D printing metals like thermoplastics: fused filament fabrication of metallic glasses, Mater. Today 21 (2018) 697–702, https://doi.org/10.1016/j.mattod.2018.07.001.
[37] H.L. Tekinalp, V. Kunc, G.M. Velez-Garcia, C.E. Duty, L.J. Love, A.K. Naskar, C. A. Blue, S. Ozcan, Highly oriented carbon fiber-polymer composites via additive manufacturing, Compos. Sci. Technol. 105 (2014) 144–150, https://doi.org/10.1016/j.compscitech.2014.10.009.
[38] L.G. Blok, M.L. Longana, H. Yu, B.K.S. Woods, An investigation into 3D printing of fibre reinforced thermoplastic composites, Addit. Manuf. 22 (2018) 176–186, https://doi.org/10.1016/j.addma.2018.04.039.
[39] N. Li, Y. Li, S. Liu, Rapid prototyping of continuous carbon fiber reinforced polylactic acid composites by 3D printing, J. Mater. Process. Technol. 238 (2016) 218–225, https://doi.org/10.1016/j.jmatprotec.2016.07.025.
[40] K. Chen, L. Yu, Y. Cui, M. Jia, K. Pan, Optimization of printing parameters of 3D-printed continuous glass fiber reinforced polylactic acid composites, Thin-Walled Struct. 164 (2021) 107717, https://doi.org/10.1016/j.tws.2021.107717.
[41] N. Maqsood, M. Rimašauskas, Influence of printing process parameters and controlled cooling effect on the quality and mechanical properties of additively manufactured CCFRPC, Compos. Commun. 35 (2022) 101338, https://doi.org/10.1016/j.coco.2022.101338.
[42] X. Tian, T. Liu, C. Yang, Q. Wang, D. Li, Interface and performance of 3D printed continuous carbon fiber reinforced PLA composites, Compos. Appl. Sci. Manuf. 88 (2016) 198–205, https://doi.org/10.1016/j.compositesa.2016.05.032.

[43] A. Diouf-Lewis, R.D. Farahani, F. Iervolino, J. Pierre, Y. Abderrafai, M. Lévesque, N. Piccirelli, D. Therriault, Design and characterization of carbon fiber-reinforced PEEK/PEI blends for fused filament fabrication additive manufacturing, Mater. Today Commun. 31 (2022) 103445, https://doi.org/10.1016/j.mtcomm.2022.103445.

[44] F. Tikhani, A. Gurbin, P. Hubert, Unveiling the impact of short fibre reinforcement and extrusion properties on microstructure of 3D printed polycarbonate composites, Addit. Manuf. 93 (2024) 104423, https://doi.org/10.1016/j.addma.2024.104423.

[45] H. Zhang, W. Sun, Mechanical properties and failure behavior of 3D printed thermoplastic composites using continuous basalt fiber under high-volume fraction, Def. Technol. 27 (2023) 237–250, https://doi.org/10.1016/j.dt.2022.07.010.

[46] D.R. Hetrick, S.H.R. Sanei, C.E. Bakis, O. Ashour, Evaluating the effect of variable fiber content on mechanical properties of additively manufactured continuous carbon fiber composites, J. Reinforc. Plast. Compos. 40 (2021) 365–377, https://doi.org/10.1177/0731684420963217.

[47] X. Tian, T. Liu, Q. Wang, A. Dilmurat, D. Li, G. Ziegmann, Recycling and remanufacturing of 3D printed continuous carbon fiber reinforced PLA composites, J. Clean. Prod. 142 (2017) 1609–1618, https://doi.org/10.1016/j.jclepro.2016.11.139.

[48] N. Maqsood, S. Mahato, M. Rimašauskas, I.I. Muna, Experimental analysis, analytical approach and numerical simulation to estimate the elastic modulus of 3D printed CCFRPC under mechanical loadings, J. Braz. Soc. Mech. Sci. Eng. 45 (2023) 1–15, https://doi.org/10.1007/s40430-023-04408-2.

[49] I.M. Alarifi, A performance evaluation study of 3d printed nylon/glass fiber and nylon/carbon fiber composite materials, J. Mater. Res. Technol. 21 (2022) 884–892, https://doi.org/10.1016/j.jmrt.2022.09.085.

[50] M. Lei, Y. Wang, Q. Wei, M. Li, J. Zhang, Y. Wang, Micromechanical modeling and numerical homogenization calculation of effective stiffness of 3D printing PLA/CF composites, J. Manuf. Process. 102 (2023) 37–49, https://doi.org/10.1016/j.jmapro.2023.07.027.

[51] N. Maqsood, G. Mordas, M. Rimašauskas, K. Skotnicová, J. Ullah, J. Gonzalez-Gutierrez, Investigation and assessment of mechanical properties of co-extrusion with towpreg continuous carbon fiber reinforced thermoplastic composites manufactured using material extrusion, Polym. Compos. (2025), https://doi.org/10.1002/pc.30004.

[52] C. Zeng, L. Liu, W. Bian, J. Leng, Y. Liu, Compression behavior and energy absorption of 3D printed continuous fiber reinforced composite honeycomb structures with shape memory effects, Addit. Manuf. 38 (2021) 101842, https://doi.org/10.1016/j.addma.2021.101842.

[53] M. Araya-Calvo, I. López-Gómez, N. Chamberlain-Simon, J.L. León-Salazar, T. Guillén-Girón, J.S. Corrales-Cordero, O. Sánchez-Brenes, Evaluation of compressive and flexural properties of continuous fiber fabrication additive manufacturing technology, Addit. Manuf. 22 (2018) 157–164, https://doi.org/10.1016/j.addma.2018.05.007.

[54] C. Marquis, R. Song, S. Waddell, A. Luong, D. Arola, Additive manufacturing with continuous ultra-high molecular weight polyethylene yarn, Mater. Des. 235 (2023) 112411, https://doi.org/10.1016/j.matdes.2023.112411.

[55] M.K. Arabi, N. Kordani, 3D-printing of Continuous Fiber : a Review of Processes , Materials and Properties, Polymer-Plastics Technology and Materials, vol. 62, 2023, pp. 1525–1559, https://doi.org/10.1080/25740881.2023.2222793.

[56] N. Maqsood, M. Rimašauskas, Fracture interface observation after the mechanical test of additively manufactured CCFRTC fabricated under the controlled air flow cooling effect, in: Proceedings of Fifth International Conference on Inventive Material Science Applications. Advances in Sustainability Science and Technology, 2023, pp. 87–95, https://doi.org/10.1007/978-981-19-4304-1_8.

[57] Y. Wang, F. Wang, Q. Xu, J. Hong, D. Wang, K. Ye, B. Gao, Design and analysis of a novel carbon fiber reinforced polymer sandwich adhesive joint, Appl. Compos. Mater. 30 (2023) 791–813, https://doi.org/10.1007/s10443-023-10113-z.

[58] D. Garoz Gómez, C. Pascual-González, J. García-Moreno Caraballo, J.P. Fernández-Blázquez, Methodology to design and optimise dispersed continuous carbon fibre composites parts by fused filament fabrication, Compos. Appl. Sci. Manuf. 165 (2023) 107315, https://doi.org/10.1016/j.compositesa.2022.107315.

[59] Q. He, H. Wang, K. Fu, L. Ye, 3D printed continuous CF/PA6 composites: effect of microscopic voids on mechanical performance, Compos. Sci. Technol. 191 (2020) 108077, https://doi.org/10.1016/j.compscitech.2020.108077.